178

ADDIS ABABA UNIVERSITY

SCHOOL OF GRADUATE STUDIES

FACULTY OF SCIENCE

DEPARTMENT OF GEOLOGY AND GEOPHYSICS

APPLICATION OF INTEGRATED GEOPHYSICAL METHODS FOR THE LANDSLIDE STUDIES OF THE BONGA TOWN

A THESIS SUBMITTED TO THE SCHOOL OF GRADUATE STUDIES OF ADDIS ABABA UNIVERSITY IN PARTIAL FULFILLMENT FOR THE DEGREE OF MASTER OF SCIENCE IN APPLIED GEOPHYSICS

BY

SENAY MEKURIA

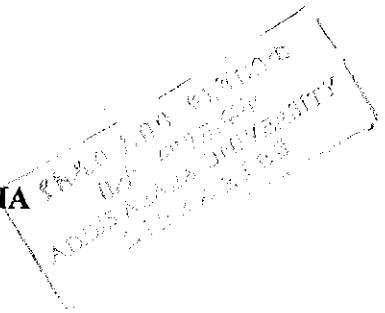

ADDIS ABABA

MARCH 2000

APPLICATION OF INTEGRATED GEOPHYSICAL METHODS FOR THE LANDSLIDE STUDIES OF THE BONGA TOWN

A thesis submitted to the School of Graduate Studies of Addis Ababa University in partial fulfillment for the Degree of Master of Science in Applied Geophysics

BY

SENAY MEKURIA

MARCH 2000

ABSTRACT

Integrated geophysical methods, particularly refraction seismic, resistivity sounding and profiling and magnetic were conducted on the landslide affected part of the Bonga town. Based on the data obtained in the survey refractor velocity and depth maps, total field magnetic and derivative maps, resistivity maps at three depth levels (AB/2=10, 45, and 100 m) and resistivity and seismic sections on selected profiles are prepared.

Tertiary volcanic, namely basalt and tuff, are the main rocks covering the Bonga town landslide area. These rocks were affected by high degree of weathering that is responsible for the formation of different grade, from weak to relatively strong basalt and fine to coarse-grained tuff. The quaternary colluvial and residual soils are found in the area covering the volcanic on the gentle to moderately sloping topography, whereas the alluvial soil is occupying the flood plains. The results of these surveys give that the saturation of unconsolidated colluvial and alluvial soil and the highly weathered volcanic formations of basaltic origin from recharge of groundwater system and the high intensity and long term rainfall in the area are determined to have a major contribution to landslide processes of the Bonga town. This high intensity and long duration rainfall by wetting and increasing the volume of the loose colluvial formation to introduce imbalance between the shearing and resisting forces that generate instability. Geophysicaly inferred structural features were delineated that have strong correlation with the occurrences and orientation of the geologically mapped active landslide scarps in the area.

The landslide area is classified into five zones based on the measured physical responses, such as resistivity, P-wave velocity and total field magnetic intensity, together with the geological observations of which Zone five (Z-5) is determined to be the most unstable one that favour landslide occurrences. Finally, some preliminary remarks and recommendations are forwarded which would help to better understand the overall landslide process in the area. The recommendations are thought to lead towards taking mitigating and controlling measures by minimizing the effect of landslide occurrences on the wellbeing of the dwellers in particular and infrastructure development of the area in general.

ACKNOWLEDGMENT

Thank God, my effort was nothing with out his blessing. I like to forward my deepest gratitude to my principal advisor Dr. Abera Alemu for his invaluable comments, concern, and proper guidance since the project proposal and critically editing the whole manuscript. I also like to acknowledge my co advisor Ato Taye Zewde for his unreserved advises in the field data collection, data processing, interpretation and editing the thesis.

I wish to tank Ato Berhanu Bekele, head of geophysics department of Ethiopian Institute of Geological surveys (EIGS) for allowing me to work on the Bonga landslide data, for using computer facilities and materials of the department and also for his technical advises.

I am also indebted to Dr. Getenet Mewa, Ato Moges Tigabe, Ato Girma Weldetinsae, Ato Kifle Damtew, Ato Nesibu Sebehat, Ato Binyam Wondirad, Ato Mamushet Zewege, Ato Shimelese Belaynehe, Ato Shimelese Fiseha, Ato Kimemu Nure, Ato Dawit Mamo, Ato Getachew Shiferaw, Ato Mengistu Zeleke and other collegues in the department whose names are not mentioned here, but their contribution in one or other way was vital for the accomplishment of this work.

In this occasion I want to say my appreciation to all my professors for making the teaching learning process attractive and potential building for a student like me who came to the academic life after long time of absence.

I also Acknowledge W/ro Melesech Demesew, W/ro Wosene Abebe and Ato Getachew Shiferaw for helping me in typing the thesis.

Table of content

Page

LIST OF FIGURES

Page

CHAPTER 1

INTRODUCTION

1.1 Location of the study area

The study area, Bonga town, where landslide phenomena occurred in August 1998 is located in the southwestern part of Ethiopia, Southern Nation Nationalities and Peoples Regional State (SNNPS). The town is an administration center of Keffa-Sheka zone. It is about 440 km from Addis Ababa through Jimma. Particularly the eastern and southeastern part of the town, Kebele 02, is affected by the landslide phenomena. The area of the landslide is bounded by 7°15'25" - 7°16'00" Latitude and 36°14'55" - 36°15'25" Longitude (Fig. 1).

1.2 Purpose and over view of the study

Geophysical methods have a significant contribution to reveal the subsurface conditions that are not observed from surface geology. Therefore, the current geophysical surveys of the Bonga town have been carried out with the following objectives:

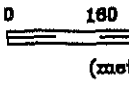

Fig.

- identify structures and buried channels, if any, which could have a relation to the landslide;
- to map the bed rock morphology of the affected site;
- determine the groundwater level of the site;
- determine the depth and nature of the bed rock (stable ground) and thickness and nature of the overburden materials;
- classify zones based on stability, bearing capacity and water tightness;
- Propose preliminary recommendations based on the results of the survey.

1.3 Regional geological setting

On the geological map of Ethiopia (Mengesha, 1996) the area under study is classified to belong to the Jimma volcanic (upper part), that consisted of trachite, ignimbrite, rhyolite, tuff with minor basalt, and the Jimma volcanic (lower part) of flood basalt with minor salic flows of late Eocene to late Oligocene age.

Whereas on the recent 1:50,000 scale engineering geological map of the area (Fig. 2) compiled in relation to the current landslide problem, basic lava flow and pyroclastic materials formed due to tertiary volcanism are indicated (Alemayehu Mulachew, personal

Fig. 2 Engir

communication). The basic lava flows are fine-grained and porphyritic basalts, while fine and coarse tuff and agglomerate represent the pyroclastic eruptions. The recent quaternary deposits are recognized as alluvial, colluvial and residual soils. Faults trending NE-SW displace the volcanic rock units with a distinct scarp zone at the eastern and southeastern of the Bonga town.

1.4 Regional hydrogeology

On the 1:2,000,000 hydrogeology map of Ethiopia (Tesfaye, 1988), the Bonga town and its surroundings are characterized by extensive acquifer, with fracture permeability of volcanic rocks (basalt, rhyolites, trachities and ignimbrites) which are found in abundance. The productivity of these acquifer systems is moderate.

As extracted from the work of Tesfaye, the water resource is wide spread with moderate to large quantities of surface water and/or ground water. Most streams are perennial. Cold springs are also common. The depth of the groundwater varies from 0 to 100 m, with static water table around 1m. Rainfall is the main recharge of the groundwater, which reaches 200-400 mm annually, being one of the highest in the country. Meanwhile, the recharge from runoff is relatively low and the discharge rate from groundwater is high.

1.5 Details of geology and landslide occurrences

1.5.1 Engineering geology

By definition landslide is a sudden or gradual rapture of rocks and their movement down slope by force of gravity (Maslov, 1987).

In the study area considered here no detailed geological and/or engineering geological works have been done previously. However, in 1999 an engineering geologist from the EIGS has carried out mapping, and as a result compiled an engineering geological map in the scale 1:2000 (Fig. 3), which is concurrent with the present geophysical survey. The study area covers 0.7 sq. km, including the geophysical surveyed area and its surrounding.

According to this study, the landslide area of the Bonga town (kebele 02) is covered by colluvial soil except the central and eastern parts, where fresh to slightly weathered and strong basalt outcrops. The colluvial soil, which is highly affected by the landslide, is formed as a result of down slope transportation by surface water. It is mainly composed of gravel (dominantly basalt), blocks of basalt and coarse tuff, loosely cemented by fine materials.

The alluvial soils cover the streambeds, particularly along the eastern stream that cross the survey area. Residual soil is the other quaternary formation without any landslide indication found in surrounding the area.

Based on engineering geological characteristics of rocks (degree of weathering, jointing and strength), basalts in the area are classified into three groups. The southwestern and partly the southern part of the landslide zone is bounded by moderately weathered, medium strong basalt. The residual soil, which has basaltic origin, is found surrounding the whole area except in the north.

The other volcanic rock- tuff, which is highly weathered, is grouped based on its grain size. The fine tuff is found out side the study area to the northwestern and southern sides.

1.5.2 History of landslide occurrences at the town of Bonga and its surrounding

According to the local inhabitants and interpretation of aerial photograph of 1967, in the Bonga town (particularly in Kebele 02) landslide has a long history that goes back to 1964 (Alemayehu Mulachew, personal communication).

The old landslide was reactivated by a high intensity rainfall that occurred in August 1998, and damaged private houses, governmental and non-governmental buildings (like the health center, prison, police department, educational department, the court and Saint Michael church). The current landslide also affected roads and water pipes.

Sporadic flows and slides can also be observed along the eastern valley slop of the Berta River and at the southwestern part of the Bonga town.

According to the above source, the Tello landslide of July 22, 1998 killed about 40 people and more than 200 people were displaced. The landslide along the Bonga-Tepi-Masha road via Alamo has disrupted the all weather road at four different places and as a result traffic has been hampered for several days.

1.5.3 The recent landslide occurrence at the Bonga town

The landslide features of the Bonga town are manifested by active scarps with cracking and subsidence (Fig. 3). There are two main land slide scarps in the area. The first starts by crossing the road to the north of St. Michael church then crossing the church floor and the compound reach the old health center. It continue to the south touching the police department then through the abandoned prison (because of the damage) up to the justice department building.

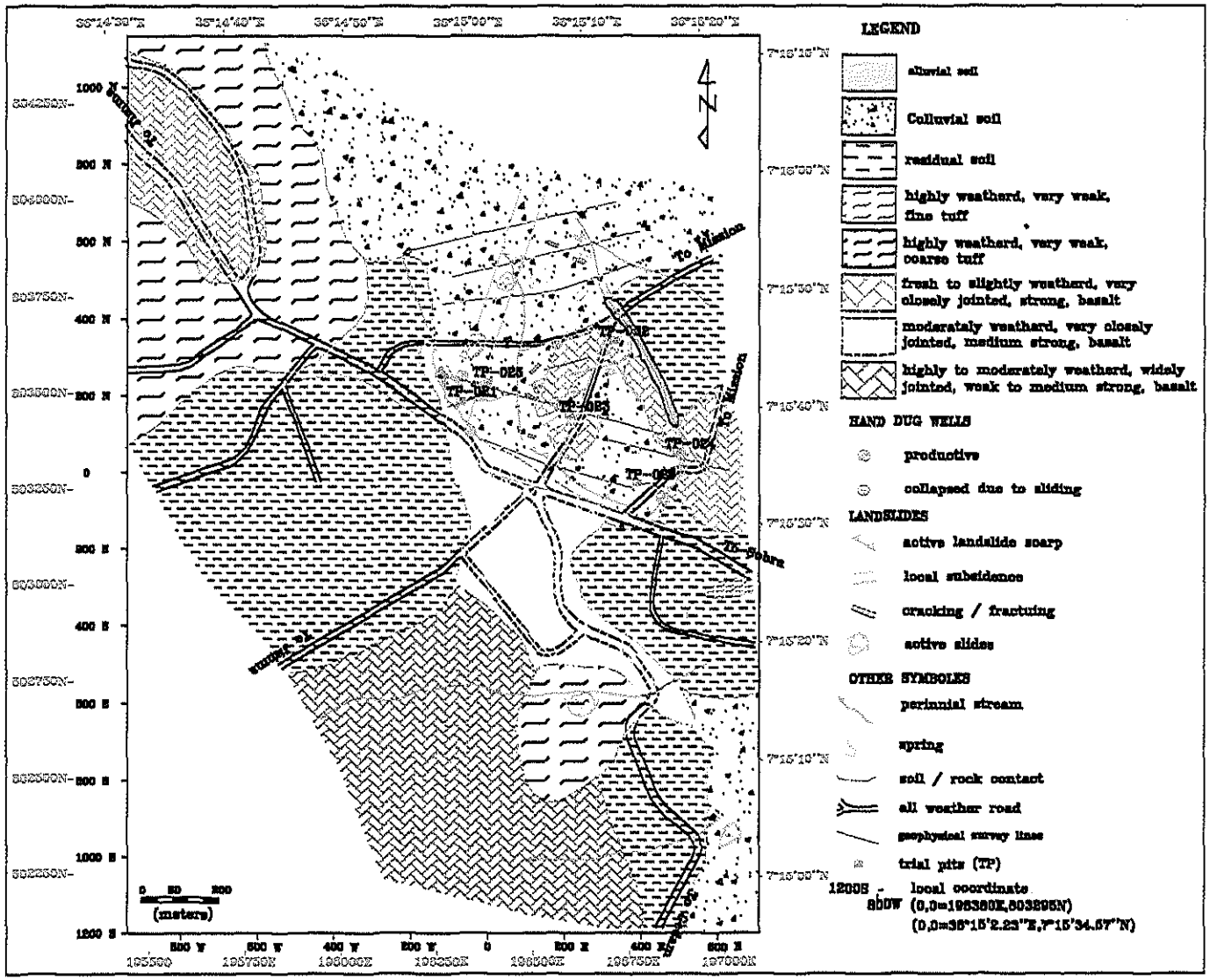

Fig. 3 Engineering Geological map of Kebele 02 and its surrounding area, BONGA (casuality area). After Alemayehu Mulachew

The second major landslide scarp (Fig. 3) starts from the front of the elementary school displacing the main road to the Sobra Mt. runs toward east affecting the concrete fence, the education department building and the near by private house compound. It further extends toward north and northwest displacing the main road to the Mission. Crossing the Mission road it has a maximum vertical displacement upto two meters that completely damage a private residence. Extending northwards it crosses the stream, and then the scarp runs parallel to the eastern bank until it disappear before reaching the main Berta river. There are several minor scarps, among them the scarp that run in the south-central part parallel to lines 6 & 7 crossing lines 6 & 12. Active slides are also observed between lines 9 and 11.

1.6 Geophysical methods for landslide studies

1.6.1 The geophysical method in general

A clear definition of the geologic problem and objectives of a particular investigation is important in determining whether certain geophysical technique should be used. Geophysical methods are primary tools for the investigation of the subsurface and are applicable to a very wide range of geological problems. Besides to their importance for exploration of natural resources, the methods are used in geo-technical investigation of sites for construction of dams, bridges, bunkers, etc. Furthermore they are applied to

environmental studies on geo-hazardous sites and selecting nuclear waste disposal sites. Though drilling is the best method for investigation of the subsurface, it is possible to minimize the cost and obtain evenly distributed information by applying geophysical techniques without disturbing the environment. Determination of the degree of fracturing in rocks has been successfully correlated with geophysical measurements in various applications (Scott et al, 1968). Geophysical methods were used for geo-technical investigation and for the study of landslides in Scandinavia countries and in the previous Soviet Union (Bogoslovsky,1977) (Sjogrern, 1984).

1.6.2 Refraction seismic method

Among the geophysical methods, refraction seismic is the best in studying areas affected by landslide. Based on the velocity contrasts, the method provides information on the thickness, water/moisture content, degree of fracturing and weathering of the unconsolidated top layer (overburden) and the underlying sound formations. In practice rocks do not behave as ideal elastic materials, but the seismic method can be used to obtain an empirical assessment of rock quality and in situ deformation modulus (Stagg et al, 1968), since an increase in degree of weathering or state of fracturing leads to a decrease in seismic velocity.

1.6.3 Electrical resistivity method

Similar to seismic refraction, electrical resistivity methods are employed in landslide studies. With this regard, the Vertical Electrical Sounding (VES) and electrical profiling are the most widely used techniques to determine both the lateral and vertical variations of the sliding mass's thickness, the depth of the water table that possibly facilitates the sliding activity. Electrical resistivity and seismic velocity have been shown to be related to porosity and broadly related to intergranular permeability with in sandstone formations (Archie, 1942; Sarmiento, 1961; Smith, 1970; Barker et al, 1973)

1.6.4 Magnetic method

Eventhough it is not a primary tool as much as seismic refraction and electrical resistivity, magnetic method is also used in the investigation of landslide prone areas. The method is used to map active landslide zones and to delineate structures such as sedimentary basins, crystalline basement, faults, etc.

CHAPTER 2

THEORY, METHODOLOGY AND APPLICATIONS OF SEISMIC REFRACTION, ELECTRICAL RESISTIVITY AND MAGNETIC METHODS

2.1 Introduction

Geophysical methods are based on the study of physical properties (velocity, density, resistivity, magnetic intensity, etc) of rocks and minerals. They are applied to solve various geological, geo-technical and other related problems. In this chapter the basic concepts of refraction seismic, electrical resistivity, and magnetic methods are summarized. For this purpose, different sources (standard geophysical text books and lecture notes, Geo 562, Geo 564 & Geo 566, on seismic, electrical & electromagnetic and gravity & magnetic methods respectively given as post graduate courses in AAU, geology and geophysics department) are used.

2.2 Seismic refraction method

2.2.1 Basic theory

The seismic method utilizes the propagation of waves through the earth. The propagation depends on the elastic properties of the rocks. A perfectly elastic body is the one that recovers completely after being deformed. Many substances, including rocks, can be considered perfectly elastic, provided that deformations are small, as in the case of seismic waves except near the seismic sources. The relation between the applied forces and the deformations are expressed in terms of stress and strain. The relation between stress and strain for homogeneous and isotropic medium are given by Hook's law as (Telford et.al., 1980):

$$\tau_{ij} = \lambda \Delta \delta_{ij} + 2\mu\varepsilon_{ij} \qquad (2.1)$$

Where τ_{ij} is stress, ε_{ij} is strain, $\Delta = \varepsilon_{xx} + \varepsilon_{yy} + \varepsilon_{zz}$ (dilatation), δ_{ij} is kroneckr delta, λ and μ are Lame's constants

If we consider a small element of volume, the six independent components of a stress can be expressed according to equation (2.1). Then wave equation could be derived from stress-strain relations and equation of motion.

By equating the net force across a cube in terms of displacement and by replacing stress components with equivalent strain components in terms of displacement, the equation of motion can be written as:

$$(\lambda+\mu)\partial\Delta/\partial x + \mu\nabla^2 u = \rho\partial^2 u/\partial t^2 \qquad (2.2)$$

$$(\lambda+\mu)\partial\Delta/\partial y + \mu\nabla^2 v = \rho\partial^2 v/\partial t^2 \qquad (2.3)$$

$$(\lambda+\mu)\partial\Delta/\partial z + \mu\nabla^2 w = \rho\partial^2 w/\partial t^2 \qquad (2.4)$$

Where u, v and w are displacement in x, y and z direction and ∇^2 is the laplacian operator.

By differentiation of equations (2.2, 2.3, and 2.4) with respect to x, y and z respectively and addition of the result gives as

$$\rho\partial^2\Delta/\partial t^2 = (\lambda+2\mu)\nabla^2\Delta \text{ or } 1/\alpha^2(\partial^2\Delta/\partial t^2) = \nabla^2\Delta \qquad (2.5)$$

where $\alpha^2 = (\lambda+2\mu)/\rho$, ρ is density of the medium through wave propagating

Equation (2.5) is the wave equation, which relates the displacement and elastic constants of the material of compression waves. It is also possible to obtain the shear-wave equation from equations (2.2, 2.3, and 2.4) after appropriate mathematical manipulation. The general form of the wave equation is

$$1/v^2(\partial^2\psi/\partial t^2) = \nabla^2\psi \qquad (2.6)$$

Solving the differential equation (2.6), the solution for plane compressional and shear wave motion in the XZ- plane is obtained as

$$\psi = Ae^{\pm i(mx+nz+\varpi t)} \qquad (2.7)$$

For compressional wave $m^2+n^2 = \varpi^2/\alpha^2$, and for plain shear-wave $m^2+n^2 = \varpi^2/\beta^2$,

where α and β are compressional and shear-wave velocities, ϖ is angular frequency, and n and m are real and imaginary constants respectively.

2.2.2 Basic principles of refraction seismic

Huygen's principle: it says "every point on a wave front can be regarded as a new source of waves that travel away from it in all directions".

Fermat's principle: it says "elastic waves travel between two points along paths requiring the least time".

If we consider a wave traveling from source S through a two layer formation having velocity V_1 and V_2 crossing the interface at A, then passing through the second layer upto G (Fig. 4)

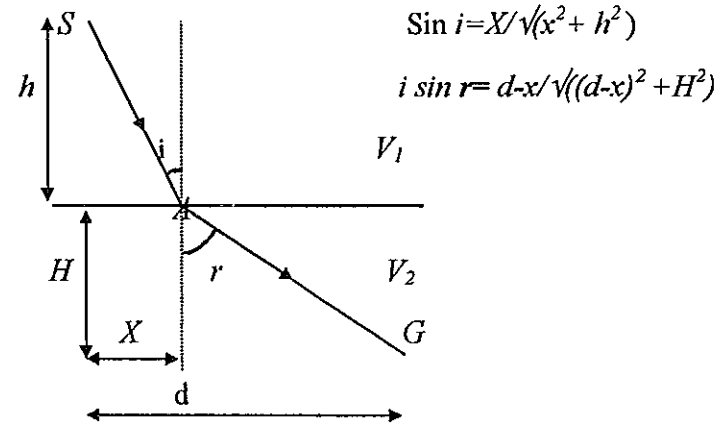

Fig. 4 Wave propagation in two layer formation

$$SA = x/\sin i = \sqrt{(x^2+h^2)}$$

$$AG = (d-x)/\sin r = \sqrt{((d-x)^2+H^2)}$$

Time taken for the ray along the path SG is

$$t = x/V_1 \sin i + (d-x)/ V_2 \sin r = [V_2\sqrt{(x^2+h^2)}+V_1\sqrt{((d-x)^2+H^2)}]/V_1V_2$$

To have the minimum time we must differentiate the above equation with respect to distance as:

$dt/dx = 0$ which gives

$$V_2x/\sqrt{(x^2+h^2)}=V_1 (d-x)/\sqrt{((d-x)^2+H^2)} \quad \text{or}$$

$$V_2 \sin i = V_1 \sin r \qquad (2.8)$$

This is the condition that should be met for the wave to travel with minimum time, and which is known as the law of refraction or *snell's law*.

When V_2 is less than V_1, r will be less than i and there is no refraction. However when V_2 is greater than V_1 and r reaches 90^0 then $i = sin^{-1}(V_1/V_2)$. For this value of r the ray is traveling along the interface, then according to the Huygen's principle it is possible to pick the ray using the sensor (geophone). The angle of incidence for which $r=90^0$ is known as the critical angle i_c, and the ray traveling along this angle is the refracted ray. Obviously, $sin\ i_c = V_1/V_2$. For angle of incidence greater than i_c, the refracted ray doesn't exist, total reflection occurs.

2.2.3 Geometry of refracted wave paths

2.2.3.1 Two layer case with horizontal interfaces

The simplest and most useful way to represent refraction data is to plot the first arrival time T versus the shot-detector distance x. In the case of a subsurface consisting of two discrete homogeneous layers, the plot consists of linear segments (Fig 5).

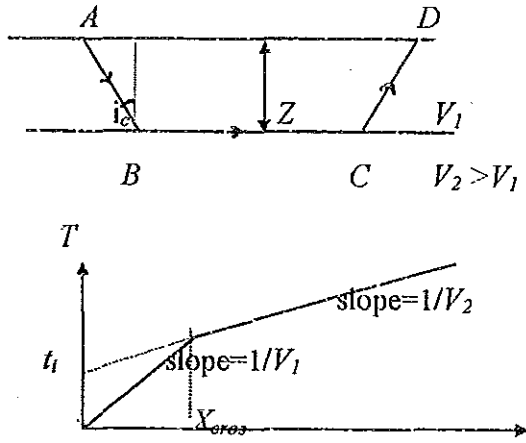

Fig. 5:(a) Travel time of direct and refracted waves from seismic shot A in a two layer system.

b) Travel-time curves for direct and refracted waves (arrivals) of the situation shown in (a)

The direct wave travels along a straight line through the top layer from source *A* to detector at D at velocity V_1. The refracted wave travels obliquely from source A down to the interface (B) at velocity V_1, along a segment of the interface (BC) at the higher velocity V_2 (for i= i_c) and backup through the upper layer at V_1.

The time taken (travel time) for the direct wave to reach D along the path AD is given by

$$T_{AD} = X/V_1$$

The total time along the refraction path *ABCD* is

$$T = T_{AB} + T_{BC} + T_{CD}$$

$$T = Z/V_1 \cos i_c + (X - 2Z \tan i_c)/V_2 + Z/V_1 \cos i_c$$

After simplification the final result will be

$$T=X/V_2 + 2Z\sqrt{(V_2^2-V_1^2)}/V_2V_1 \qquad (2.9)$$

On a plot of T versus X, this is the equation of a straight line, which has a slope of $1/V_2$ and intercepts the T axis $(x=0)$ at a time

$$T_i=2Z\sqrt{(V_2^2-V_1^2)}/V_2V_1 \qquad (2.10)$$

where T_i is known as intercept time.

At a distance X_{cros} (Fig. 5b) the two linear segments cross each other. At distance less than X_{cros} the direct wave traveling along the top velocity layer (V_1) reach the detector first (Fig.5a). At greater distance the wave refracted by the interface arrives before the direct wave. For this reason, X_{cros} is called the cross over distance.

The depth Z to the interface can be calculated from the intercept time by the use of equation (2.10) as:

$$Z= T_i V_2V_1/2\sqrt{(V_2^2-V_1^2)} \qquad (2.11)$$

T_i can be determined graphically as shown in (Fig. 5) or numerically from the relation

$$T_i = T - X/V_1 \qquad (2.12)$$

The depth can also be expressed in terms of X_{cros}, making the use of the fact that the times for the direct wave *and* refracted wave are equal at X_{cros}. This can be expressed as:

$$Z= X_{cros}\sqrt{(V_2-V_1)}/2\sqrt{(V_2+V_1)} \qquad (2.13)$$

2.2.3.2 Three layer case with horizontal interface

When all beds are horizontal equation (2.8) can be generalized to cover the case of more than one refracting horizon. For three layer case (Fig. 6) $V_3>V_2>V_1$ and sin i_1/ V_1= sin i_c/ V_2=1/ V_3

$$T= X/V_3 + 2Z_2 \cos i_c /V_2 + 2Z_1 \cos i_1/V_1 \quad \text{or}$$

$$T=(X/ V_3)+T_2 \qquad (2.14)$$

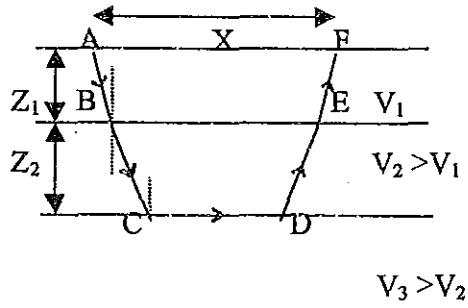

Fig. 6 Travel path of direct and refracted waves from a seismic source situated at the surface of a three-layer system

2.2.3.3 Multi-layer case with planer interfaces

In general the travel time T_n of a ray critically refracted along the top surface of the n^{th} layer is given by

$$T_n = (X/V_n) + \sum_{j=1}^{n-1} 2Z_j \cos i_j/V_j \qquad (2.15)$$

where $i_j = \sin^{-1}(V_j/V_n)$

2.1.3.4 Dipping-layer case with planer interfaces

In the case of dipping refractor the travel time equation is with additional unknown parameter the dip angle, and the velocity obtained from the travel time curve is apparent velocity. The velocity from the direct and reverse shot is also different. Considering all these the general form of equation for the travel time t_n of a ray critically refracted in the n^{th} dipping refractor is given by

$$t_n = (X \sin\beta_n/V_n) + \sum_{i=1}^{n-1} \{(h_i (\cos\alpha_i + \cos\beta_i))/ V_i\} \qquad (2.16)$$

where h_i is the vertical thickness of the i^{th} layer beneath the shot, v_i is the velocity of the ray in the i^{th} layer, α_i and β_i are the angles with respect to the vertical made by the down going and up going ray of the i^{th} layer and x is the offset distance between the source and the detector.

2.1.4 Refraction seismic interpretation techniques

2.1.4.1 The T-0 method

The T-0 method (Gurvich, 1972) is refractor velocity determination technique. The refractor velocity is determined from the inverse slope of the residual time curve. The residual time curve can be obtained using the formula:

$$\theta(x) = t_d(x) + (T - t_r(x)) \qquad (2.17)$$

where $t_d(x)$ and $t_r(x)$ are the direct and reverse travel times at point x on the profile and T is the reciprocal time. Then the boundary velocity is determined from each linear segments of the residual time curve as

$$V_b = 2\,\Delta X / \Delta\theta(x) \qquad (2.18)$$

Depth determination at the impact points are made by phantomming (finding of the true intercept time (t_i) by extrapolating the time curve to the impact point keeping parallel with the travel time curve from the offset shots), that simplify depth determination at $x=0$.

2.1.4.2 The ABC method

Depth to the refractor surface is determined by applying the ABC method. The method involves a summation of overlapping arrival times of critically refracted waves at a common surface point, from two impact points minus the reciprocal times (Fig. 7).

$$t_0(x) = t_d(x) - (T - t_r(x)) \qquad (2.19)$$

where $t_0(x)$ is intercept time at the geophone station.

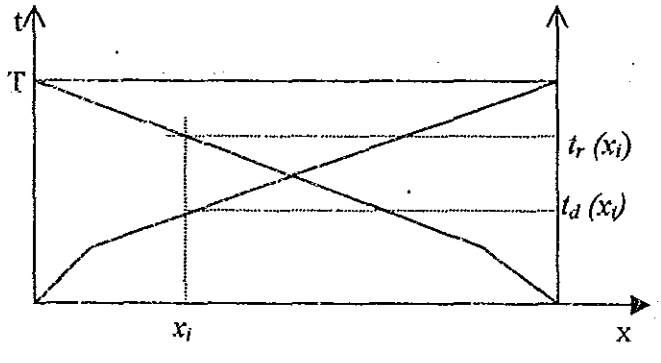

Fig. 7. Schematic illustration that show how to determine $t_0(x)$

Velocity of the overburden formation is determined from the general formula:

$$V_{av} = \sum_{i=1}^{n} h_i / \sum_{i=1}^{n} (h_i/V_i) \qquad (2.20)$$

where h_i is thickness of the i^{th} layer and V_i is velocity of the i^{th} layer

Then using boundary velocity (V_b), intercept time (t_0) and the average velocity of the

overlaying layer (V_{av}) depth to the main refractor (H) could be calculated by the formula:

$$H = t_0(x) / [\sqrt{((1/V_{av}^2) - (1/V_b^2))}] \qquad (2.21)$$

2.3 Electrical resistivity method

2.3.1 Basic idea and scope

In the electrical resistivity method, artificially generated direct commutated or low frequency alternating currents are introduced into the ground by means two current electrodes connected to the terminals of a portable source of e.m.f. The resulting potential distributions or potential differences on the ground are mapped by means of two non-polarizable potential electrodes.

The subsurface rock resistivity variations affect the electrical current flow and this intern affects the distribution of surface electrical potentials.

Deviations from the pattern of potential differences expected from a homogeneous ground provide information on the form and electrical properties of the subsurface inhomogeneties. The method has been used mainly in the search for water bearing formations, in stratigraphic correlation.

2.3.2 Electric conduction in continuous isotropic media

Considering a continuous current flow in an isotropic homogeneous medium, according to ohm's law electric field E and current density J are related as

$$J = \sigma E \quad \text{or} \quad E = J\rho \qquad (2.22)$$

where σ - conductivity of the medium and

ρ - resistivity of the medium (inverse conductivity)

The electric field is the gradient of

$$E = -\nabla V \qquad (2.23)$$

Thus, by combining equations 2.22 and 2.23, one obtains,

$$J = -\sigma \nabla V \qquad (2.24)$$

The divergence of current density is equivalent to the time rate of accumulation of charge density; Q, which can mathematically be expressed as

$$\nabla . J = \partial Q / \partial t \qquad (2.25)$$

In regions of finite conductivity, charge does not accumulate to any extent during current flow, hence;

$$Q = 0$$

and $\nabla . J = 0$ (2.26)

Substituting the expression for J in equation 2.24 into equation 2.26 results in

$$\nabla . (\sigma \nabla V) = 0 \qquad (2.27)$$

Applying the identity $(A \nabla B) = \nabla A \nabla B + A \nabla^2 B$ to equation 2.24 one can arrive at

$$\nabla \sigma \nabla V + \sigma \nabla^2 V = 0 \qquad (2.28)$$

If σ is a constant, the first term in equation (2.25) vanishes, where the resulting expression can be given as

$$\nabla^2 V = 0 \qquad (2.29)$$

Equation 2.26 represents Laplace's equation and signifies that the electric potential V is harmonic. This gives freedom to subdivide the subsurface in each electrically homogeneous and isotropic layers based on the potential differences they generate. This possibility is because of the fact that the total potential can be decomposed into its component parts as it is harmonic satisfying Laplace's equation.

2.3.3 Potential due to a point current electrode on homogeneous earth

In the case small electrode is buried in homogeneous and isotropic ground, the current circuit is completed through another electrode on the surface where its influence is

negligible, the potential will be a function of r (distance between the electrode and the point of consideration). Laplace equation in spherical coordinates is suitable for this condition and can be expressed as

$$\nabla^2 V = d^2 V/dr^2 + 2dV/rdr = 0 \qquad (2.30)$$

Multiplying by r^2 and integrating gives

$$dV/dr = A/r^2 \qquad (2.31)$$

Integrating again gives

$$V = -A/r + B \qquad (2.32)$$

where A and B are constants determined by the boundary conditions.

i) i) $V \to 0 \quad as \quad r \to \infty$

i.e. $B=0$

ii) The current flows radially out ward in all directions from the point electrode. Thus, the current passing through a spherical surface of radius r is given by

$$I = 4\Pi r^2 J$$

Using equation (2.22) (2.23) and (2.31)

$$I = -4\Pi r^2 \sigma dV/dr = 4\Pi \sigma A$$

So that $A = -I\rho/4\Pi$

Then inserting the expression of A in equation (2.32)

$$V = I\rho/4\Pi r \quad or \quad \rho = 4\Pi rV/I \qquad (2.33)$$

But if the electrode is on the ground surface (Fig. 8), additional conditions should be satisfied, i.e.

i) The potential at the surface has to satisfy the relation.

$dV/dz = 0$ at $Z = 0$ Since $\sigma_{air} = 0$

$$\partial v/\partial z = \partial/\partial z\,(-A/r) = -\partial/\partial r(A/r)\partial r/\partial Z$$

$$= Az/r^3 = 0 \quad \text{at} \quad Z = 0$$

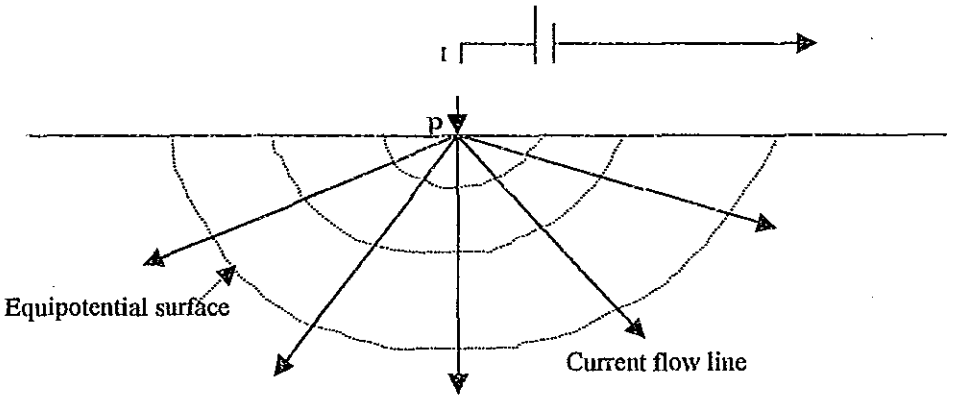

Fig. 8. Current flow from a single source electrode.

ii) Now all the current flows through a hemispherical surface in the lower medium, so in this case a will be half of the previous case (the point source in the ground)

$$A = -I\rho/2\pi$$

Consequently

$$V = I\rho/2\pi r \qquad or \qquad \rho = 2\pi rV/I \qquad (2.34)$$

In practice two electrodes are used, one positive (A) sending current in to the ground, and the other negative (B), collecting the returning current (Fig. 9).

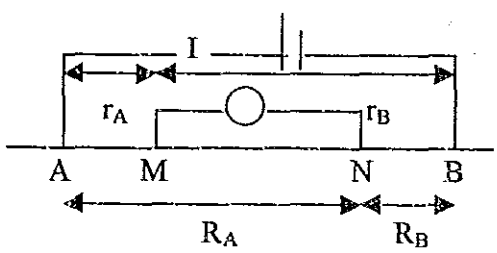

Fig. 9. Generalized form of electrode configuration used in resistivity measurement.

The total potential at any point M in the ground will then be

$$V_M = I\rho\,(1/r_A - 1/r_B)/2\pi$$

Similarly, the potential at electrode N will be

$$V_N = I\rho\,(1/R_A - 1/R_B)/2\pi$$

Finally, the potential difference between electrodes m and N will be

$$V_{MN} = (I\rho/2\pi)\{(1/r_A) - (1/r_B) - (1/R_A) + (1/R_B)\}$$

There are different types of configurations used in resistivity measurements with their own advantages and disadvantages. Wenner, Schlumbreger, dipole-dipole, and Gradient arrays are among the common electrode configurations.

2.3.4 Potential distribution on horizontally stratified earth

To know the measurement and interpretation of electrical resistivity sounding on stratified subsurface, it is important to find a relation for the electrical potential at the surface of the earth, by considering the potential field due to a single point source of current. According to Stefanescu et al (1930) the potential will be derived based on the specifications.

1) The subsurface consists of an infinite number of layers with finite thickness separated by horizontal planes; the deepest layer extends to infinite depth.

2) Each of the layers is electrically homogeneous and isotropic.

3) The field is generated by a point source of current located at the surface of the earth.

4) The current emitted by the source is direct current.

It is discussed that the electrical potential in direct current satisfies Laplace's equation. In this case the potential field must have cylindrical symmetry in line through the current

source. Then it is appropriate to use Laplace's equation in cylindrical coordinate which given as

$$\partial^2 V/\partial r^2 + (1/r)\,\partial V/\partial r + \partial^2 V/\partial z^2 \qquad (2.36)$$

Using the procedure of differential equation theory of Bessel function and that of a potential at any point the general solution of equation (2.29) will be

$$V_i = \rho_1 I/2\pi \int_0^\infty [e^{-\lambda z} + \theta_i(\lambda) e^{\lambda z} + X_i(\lambda) e^{-\lambda z}]\, Jo(\lambda r)\, d\lambda \qquad (2.37)$$

which is known as the Stefanescu integral. Where the subscript i refers to several layers in the subsurface

λ is arbitrary constant

$\theta_i(\lambda)$ & $X_i(\lambda)$ are arbitrary functions of λ

J_o is the Bessel function of order zero

ρ_1 is the resistivity of the homogeneous earth

I is the current intensity

In the case of a potential field set up by a single point source of current at the surface of horizontally stratified earth, the following boundary conditions must be satisfied:

i) At each of the boundary planes in the subsurface the potential must be continuous.

$V_i = V_{i+1}$ at $Z = h_i$

ii) At each of the boundary planes in the subsurface the vertical component of the current density must be continuous.

$(1/\rho_i)\partial V_i/\partial z = (1/\rho_{i+1})\partial V_{i+1}/\partial z$ at $Z = h_i$

iii) At the surface the normal current density must be zero, except in the infinitesimal neighborhood of the source (since σ air = 0 and according to condition ii)

This implies $\theta(\lambda) = X(\lambda)$

iv) Near the current source the potential must be finite.

v) At infinite depth the potential must approach to zero.

Using these boundary conditions a set of 2n equations with 2n unknown functions of $\theta(\lambda)$ *and* $X(\lambda)$ are produced

From this system of equations the solution of θ_i is obtained by the application of Creamer's rule. According to this rule, θ_i is determined as the quotient of two determinants. For example for two layer case

$$\theta_1(\lambda) = K_1 e^{2\lambda h}{}_1 / K_1 e^{-2\lambda h}{}_1 \qquad (2.38)$$

where K_1 is the reflection coefficient expressed as

$$K_1 = \rho_2 - \rho_1 / \rho_2 + \rho_1$$

The potential on the surface of stratified earth (z=0), the Stefanescu integral reduced to

$$V = I\rho/2\pi \int_0^{\infty} \{1+2\ \theta_1(\lambda)\}\ J_0(\lambda r)\ d\lambda \quad or$$

$$V = I\rho/2\pi \int_0^{\infty} K(\lambda)\ J_0(\lambda r)\ d\lambda \qquad (2.39)$$

where $K(\lambda)$, which was first introduced into resistivity sounding theory by Slichter (1933), is called the Slichter Kernel function, and $\theta_1(\lambda)$ is the Stefanescu Kernel function.

2.3.5 The apparent resistivity function

The resistivity obtained by inserting the potential difference and current measured using any electrical configuration, in the corresponding array expression, which is derived by assuming homogeneous earth is apparent resistivity.

2.3.6 Calculation of apparent resistivity from field observation

As illustrated in Fig. 7a, using symmetrical configuration, particularly Schlumbreger array, and the potential difference between the measuring electrodes (M & N) for a homogeneous earth is

$$\Delta V = (I\rho/\pi)\ ((1/s-b)-(1/s+b)) \qquad (2.40),$$

Where s is half of the current electrode separation AB; b is half of the measuring electrode separation MN; ρ is apparent resistivity of the medium

By rearranging the above equation the apparent resistivity for Schumberger array is given by

$$\rho_{ap\,sch} = (2\pi s\,(s^2 - b^2)/\,4bs)\,\Delta V / I \qquad (2.41)$$

where the relation $2\pi s\,(s^2 - b^2)/4bs = K$ is known as the geometric factor

2.3.7 Apparent resistivity transform function and its relation with apparent resistivity

For Schulumberger array, the resistivity transform $T(\lambda)$ first introduced by Koefoed (1970), defined interms of resistivity, ρ and slichter Kernel function $K(\lambda)$ as

$$T(\lambda) = \rho K(\lambda) \qquad (2.42)$$

$T(\lambda)$ has an important role in modern theory of the interpretation of resistivity sounding, therefore, it is basic to know the relation between the apparent resistivity function and apparent resistivity transformation function. To derive their relation, assuming infinitesimal distance between the potential electrode in equation (2.42) $(s^2 - b^2)/\,4bs$ reduces to $s/4b$ which implies, that the electric field intensity can be considered to be constant between measuring electrodes. The potential gradient $\Delta V/2b$ can then be replaced by a differential quotient $2(\partial V/\partial r)_{r=s}$.

Therefore, equation (2.41) reduces to $\rho_{ap\,sclh} = -2\pi s^2 / I\{(\partial V/\partial r)_{r=s}\}$

By substituting the expression for $\theta_1(\lambda)$ as shown in equation 13 (after applying Lipschitz integral) into equation (2.42) and during the differentiation which affect the Bessel function as

$\partial/\partial x\ (J_0(x)) = -J_1(x)$, which is Bessel function of order one then the apparent resistivity took the from:

$$\rho_{ap\ schl} = \rho_1 + 2\rho_1 s^2 \int_0^\infty \theta_1(\lambda) J_1(\lambda s)\, \lambda\, d\lambda, \quad \textit{or using equation (2.43)}$$

$$\rho_{ap\ schl} = \rho_1 + s^2 \int_0^\infty [T(\lambda)-\rho_1] J_1(\lambda s)\, \lambda\, d\lambda \qquad (2.44)$$

2.3.8 Resistivity profiling

Usually resistivity profiling is done to have a qualitative information about the survey area. For engineering geology and occasionally in mining geology it is used to investigate the over burden resistivity variation, and to have a rough estimation of thickness up to the bedrock. In groundwater exploration it has great contribution to study the aquifer zone.

Another important application of profiling is for identification of vertical structures with their large resistivity contrast, such as fault contacts, dikes, shear zones and group of veins, mostly cases of mineral exploration areas.

In the case of simple structures, one or two vertical boundaries or contacts, the image method is used to determine the apparent resistivity. The reflection coefficients that depend

on the resistivity of the medium encountered and the electrode configuration used are the main factors to determine the potential difference.

The response of profile curves in different geology varies based on the array used and the geological structure encountered. (Keller et al, 1966).

2.3.9 Interpretation of vertical electrical sounding (VES) data

There are two types of VES interpretation: direct and indirect. The indirect method comprises curve matching between the VES curves obtained from the field and VES curves computed for assumed theoretical models and the auxiliary point method, whereas the direct method comprises automatic forward and inversion techniques.

2.3.9.1 Curve matching by master curves

This method involves a comparison of measured curve with a set of theoretically calculated master curves. The theoretical master curves are plotted resistivity verses electrode separation on a logarithmic graph paper with modules of 62.5 mm. There are many albums of theoretical curves computed using different techniques. Some of them are Mooney and Wetzel (1956) computed using numerical integration. Orellana and Mooney (1966), Rijkswaterstaat (1969) used the image point computation method. Computation by

decomposition into partial fractions was used to produce the collection of the companies Generale de Geophysique (1955). This technique is practicable only when the number of layers are small, say up to four. Even for four-layer case the number of reasonable parameter combination is so large and the collection of curves so bulky that interpretation by matching become impractical. Therefore for a large number of layers it s virtually impossible. Currently this type of curve matching technique is obsolete.

2.3.9.2 Partial curve matching

This technique requires matching of small segments of the field profile with theoretical curves (master curves and auxiliary curves) for two or if possible, three horizontal layers. Generally one would start from the left-hand (small spacing) side of the curve and much successive segments toward the right (large spacing). When a portion of the field curve is reasonably matched in this way, all the layers in this segment are lumped together and assumed to have an effective resistivity ρ_e and depth z_e. This lumped layer is used as a surface layer and the next portion of the field curve is interpreted in a similar way. Here we discuss the two layer partial curve matching. This method requires two layer master curve and four auxiliary curves for curve types *H*, *Q*, *A* and *K*. The interpretation procedure is:

1. Trace the field curve on a transparent paper which is scaled the same as the master curve.

2. Match the left hand portion of the field curve to a master curve. From this match, trace the origin of the master curve (first cross) which designate (h_1,ρ_1) and the ratio of ρ_2/ρ_1.

3. Superimpose the transparent paper on the auxiliary curve of the right type. Keep axes parallel at all times (on master curve and auxiliary curves). For Q and H type curves, place the first cross over the coordinate origin of the auxiliary curve. For A and K type curves, place the first cross over the left-hand vertical axis of the auxiliary curve, corresponding to the value of ρ_2/ρ_1.

4. Select the curve on the auxiliary curves which correspond to ρ_2/ρ_1 and trace this curve on the transparent paper starting the first cross.

5. Superimpose the transparent paper on the master curve again, now to fit the next part of the field curve by sliding the transparent paper on the origin of the master curve along the auxiliary curve previously drawn.

6. On the transparent paper mark the position of the second cross and the resistivity ratio which fit the second part of the field curve on the master curve sheet. The resistivity ratio gives $\mu_e = \rho_3/\rho_e$. The second cross gives (he,ρ_e).

7. Superimpose the field curve again on the auxiliary curve; place the first cross on the same position as step 3. The position of the second cross lies on a dashed line which gives as $v_2=h_2/h_1$.

8. In the same way the above procedure will continue until the whole field curve is completely matched.

The auxiliary point chart method of approximate interpretation was first published by Ebert (1943) and partially utilized by Humel. A lot of modifications are done on this method by many authors. Orelane & Mooney (1966) Homilius (1961), Zohdy (1965), Battacharya and Patra (1968).

2.3.9.3 Resistivity Interpretation through 1-D Modeling

The objective of 1-D Modeling of an apparent rsistivity curve for certain DC sounding arrays is to arrive at $\rho(z)$, given ρ_a verses depth, under the measurement location. This can be done either through direct transformation or through interactive curve fitting procedures that are of a least square nature. Since Slichter (1933), Pekeris (1940), Van Nostrand & Cook (1955), Koefoed (1968), presented their work based on the variation of resistivity with depth is stepwise.

Recently more powerful inversion processes have been applied to solve the problem in different approach. Some of them are Marquardt (1963), Meinardus (1970), Inman et al (1973), Marsden (1973), Zohdy (1974), Inman (1975), Johansum (1977) & Cecehi et al (1977).

Of all inversion techniques ridge regression inversion is confirmed to be the best for solving resistivity problem.

2.3.10 Resitivity inversion with ridge regression

Inversion of resitivity sounding in kernel domain or apparent resistivity domain is performed in a least square sense to fit a theoretical or calculated curve to the observed or real data.

$$o(p,x)_i = c(p^0,x) + \Sigma\, \partial/\partial p_j\, [\, c(p,x)\,]\,(p_j - p^0_j) \quad \text{for j = 1, n and i=1, m} \qquad (2.37)$$

where $o(p,x)_i$ is the ith observation at the electrode space x and p is the unknown parameter.

$c\,(p^o,x)_i$ is calculated function value for x and p^o.

p^o is the initial estimate for unknown parameter set

$(p_j - p^0_j) = \Delta p_j$ is the linear estimate of the correction needed in the jth unknown parameter.

Rewriting equation (2.37) in matrix representation

$$\Delta G = A\, \Delta p \qquad (2.38),$$

where $\Delta G_i = o(p,x)_i - c(p^0,x)_i$

$A_{ij}\, \partial c(p^0,x)_i/\partial p_j$ is the system matrix

After some algebraic rearrangement equation (2.38) becomes

$$\Delta p = (A^T A)^{-1} A^T G \qquad (2.39)$$

This is the least square inverse, where A^T is transpose of derivative matrix A.

When $A^T A$ is singular, the average difference between Δp true and Δp estimated become very large. Hence the need to introduce a biased estimator in the least square inverse,

$$\Delta p = (A^T A + KI)^{-1} A^T \Delta G \qquad (2.40)$$

is the ridge regression estimation of Δp. Where I is the identity matrix. Increasing the ridge regression estimator by a factor K will result in the stability of $(A^T A + KI)^{-1}$, in the case of very small Eigen values (Moges Tigabe, 1991).

The advantage of ridge regression as the finding of Marqurdt is, its fastly convergence with small Eigen values.

2.4 Magnetic method

2.4.1 Basic concepts

With in the vicinity of a bar magnet a magnetic flux is developed which flows from one end of the magnet to the other. The points within the magnet where the flux converges are known as the poles of the magnet.

The force F between two magnetic poles of strength m_1 and m_2 separated by a distance r is given by

$$F=\mu_o m_1 m_2 /4\pi\mu_R r^2 \qquad (2.41)$$

Where μ_o is magnetic permeability of vacuum and μ_R is relative magnetic permeability of medium separating the poles.

The force is attractive if the poles are different in sign, repulsive if they are of like sign. The magnetic field B due to a pole of strength m at a distance r from the pole is defined as a force exerted on a unit positive pole at that point.

$$B = \mu_o m/4\pi\mu_R r^2 \qquad (2.42)$$

Magnetic fields can be defined in terms of magnetic potential. For a single pole of strength m_1, the magnetic potential V at a distance r from the pole is given by

$$V=\mu_o m/4\pi\mu_R r \qquad (2.43)$$

The magnetic field component in any direction is then given by the partial derivative of the potential in that direction.

To define magnetic parameters in the SI system of units, consider the flow of current through a coil of several turns that produce magnetic flux B from a magnetizing force H. The magnitude of H is proportional to the number of turns in the coil and the strength of a current and inversely proportional to the length of a wire. So that H is expressed in Am^{-1}. The magnetic field B measured over the area perpendicular to the direction of flow is proportional to H with proportionality constant magnetic permeability. From Lenz's law B

is expressed in volt sm^{-2} or (Weber (Wb) m^{-2}) which is designated by the tesla (T). The c.g.s unit of magnetic field strength is the Gauss (G), equivalent to 10^{-4} T. There is sub unit the nano-Tesla (nT) which is equivalent to 10^{-9} T. The c.g.s system employs the numerical equivalent gamma (γ), equal to 10^{-5} G.

Magnetic moment: - Common magnets exhibit a pair of poles and they are referred as dipoles. The magnetic moment M of a dipole with poles of strength m and a distance L apart is given by

$$M = mL \qquad (2.44)$$

The magnetic moment of a current carrying coil is proportional to the number of turns in the coil. Therefore, magnetic moment is expressed in Ampere m^2.

Intensity of magnetization: - When a material is placed in a magnetic field it acquires magnetization by induction in the direction of the field. This phenomenon is known as induced magnetization or magnetic polarization. The intensity of magnetization is defined as the dipole moment per unit volume of a material, given by

$$J = M/V \qquad (2.45)$$

Therefore intensity of magnetization is expressed in Am^{-1}.

Magnetic susceptibility: - The induced intensity of magnetization is proportional to the strength of the magnetizing field B of the inducing field.

$$J \alpha B \qquad \Rightarrow \qquad J = kB \qquad (2.46)$$

The proportionality constant k is known as the magnetic susceptibility of the material. Since J and B are measured in the same unit, susceptibility is dimensionless. But this parameter k is very important in exploration geophysics because by measuring the susceptibility of samples in the laboratory it is helpful to do quantitative interpretation by modeling.

2.4.2 Geomagnetic field

Eventhough in different proportion, the cause of geomagnetic field is attributed to internal and external origins. The geomagnetic field is geometrically more complex than the gravity field variation in both orientation and magnitude.

2.4.2.1 Geomagnetic field of internal origin

This part of the geomagnetic field is grouped into two: the main field (dipole field) and the variations of the main field due to the rock magnetism.

A dynamo action produced by the circulation of charged particles coupled with the convection (fluid motion) of the outer core of the earth, influenced by the earth's rotation that give the patterns involved in the generation of the main magnetic field.

The evidence from the seismic data that *S-waves* do not propagated in the outer core and the abundance of *Fe* and *Ni* occurrence in the meteorites which account for iron is a good conductor and its density is just about right for the total mass of the earth. This strongly supports that the liquid iron core is the origin of the main geomagnetic field.

The circulation patterns with in the core are not fixed and change slowly with time. This is reflected in a slow, progressive temporal change in all the geomagnetic elements and is known as secular variation. An example for such variation is the gradual rotation of the north magnetic pole around the geographic pole.

a) Elements of the main field

At any point of the earth's surface a freely suspended magnetic needle will assume a position in space in the direction of the geomagnetic field. Generally it will be at an angle to both the vertical and geographic north. The total field vector B has a vertical component Z and a horizontal component H in the direction of magnetic north. The dip of B from the horizontal is inclination *(I)* and the horizontal angle between geographic and magnetic north is the declination *(D)* (Fig. 6).

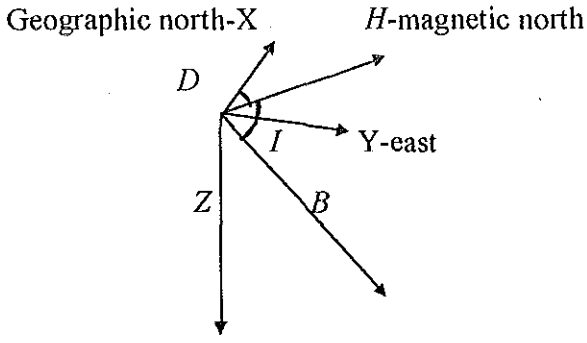

Fig. 10. Elements of the geomagnetic field.

B varies in strength from about 25,000 nT in equatorial regions to about 70,000 nT at the poles. About 90% of the earth field can be represented by the field of a theoretical magnetic dipole at the center of the earth inclined at about 11.5^0 to the axis of rotation.

By the technique of successive approximations of the observed field which is known as spherical harmonic analysis, the formula of the International Geomagnetic Reference Field (IGRF) is computed to define the theoretical undisturbed magnetic field at any point of the earth's surface. In magnetic surveying, the IGRF is used to remove from the magnetic data those magnetic variations attributable to this theoretical field.

b) Variation of the main field (local anomalies)

Ferromagnetic rocks and minerals present in the near surface of the crust produce a magnetic field known as rock magnetism. It is obtained by subtracting the main field (B_o) and any external fields (diurnal corrections) from the observed total field (B_{obs}) as

$$\Delta B = B_{obs} - B_o - \delta B, \qquad (2.47)$$

where ΔB is anomalous field due to rock magnetism, B_{obs} is total field observed at any point on the surface, B_o is the main field determined from IGRF maps, and δB is diurnal correction. It is much smaller than the main field, but it is complex due to the nature, its depth, magnitude, shape and position of the causative body.

2.4.2.2 Geomagnetic field of external origin

Geomagnetic field of external origin comprises about 1% of the total geomagnetic field. The cause of this field is flow of charged particles within the ionosphere towards the earth, in large towards the magnetic poles and also due to the field effect of the sun around the moon. This cause a diurnal variation from 20 - 80 nT on smooth and regular basis but some times it reaches an amplitude of 1000 nT known as magnetic storm. Magnetic survey should be abandoned on the time of magnetic storm.

CHAPTER 3

DATA ACQUISITION, PROCESSING AND PRESENTATION

3.1 Introduction

Geophysics is a vast and highly developed earth science, with long and tiresome processes that pass through from field observation to report writing. In this study three geophysical methods namely resistivity that include VES and horizontal profiling, refraction seismic and magnetic were conducted. The geophysical crew from the Geophysics Department of Ethiopian Institute of Geological Surveys (EIGS) has done the field data collection. The author of this thesis has participated in 30% of the data collection, while the remaining 70% of the field data were obtained from the EIGS field crew.

3.2 The seismic data acquisition, processing and presentation

3.2.1 Instrumentation

The refraction seismic survey was conducted with 24 - channel microprocessor based, Swedish made, ABEM TERRALOCK MK-III seismograph. Geophones PE-3 (10 Hz) type

were used for the reception of signals. A 7-kg sledgehammer was used to generate seismic waves. Hammering was made on a hard plastic plate. In addition, 12 V car battery was employed as an external power supply for the seismic unit.

The seismograph has two disc drives, which are used for the storage of the seismic traces. It also has a semi automatic facility to magnify and filter (if necessary) the weak signals. There is also an option to pick first arrivals (that is used in refraction seismic) automatically or manually in digital or analogue form. Then the digital and/or the seismic trace could be printed using the interface cable.

3.2.2 The refraction seismic data acquisition

The refraction seismic data collection is performed using the instrument setup (Fig. 11c) where 24 geophones are arranged in 5 m spacing that cover 110 m (one spread). Five shots per spread were utilized. These are the direct offset shot, the direct shot, the central shot, the reverse shot and the reverse offset shots. The distance between consecutive shots was kept constant 55 m. This arrangement is used to have two geophones overlap reading, which replace the 23^{rd} and 24^{th} geophones in the first spread by the 1^{st} and the 2^{nd} geophones in the second spread.

A sledgehammer was used as the only energy source although dynamite is known to be a better energy source, particularly for larger depth investigations. However, in addition to

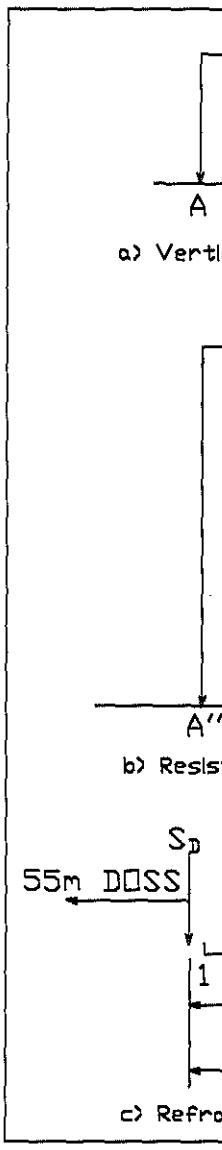

Fig.

that the area is a settlement site so it is prone to property and life damages, it is believed that dynamite aggravates the landslide in the area. With refraction seismic survey a total of 45 spreads that cover 5.27 km along 14 survey lines were conducted (Fig. 13 & 14).

3.2.3 The refraction seismic data processing and presentation

The frequency filtering option of the instrument was used to eliminate unwanted signals. The seismograms were produced using the instrument's internal computer and further the first arrivals were picked manually or using auto pick option of the seismograph. Then the first arrival times verses the shot-geophone distances were plotted along profiles considered.

After drawing a horizontal line through the reciprocal time (the actual time from impact point to impact point for waves propagating via refractor), parallelism between the various velocity segments corresponding to same horizon have been checked.

The travel time curves (time distance curves) are then examined to find the likely number of layers, the apparent velocities in them and the positions of apparent pick points.

The depth analysis and the velocity distribution in the bottom refractor were carried out using T-0 method.

There is no velocity coverage of the overburden in the time distance graph (the travel time

curves from the second layer do not overlap even over short sections of the profiles). So that an estimate of the second layer velocity was made, by taking the harmonic mean of the apparent up dip and down dip velocities.

The first layer velocity was determined by averaging the inverse slope of the direct and reverse recordings.

Then the depth determinations at the impact points and through out the main refractor, the true intercept time at the impact point and the average velocity of the overburden formation were carried out applying appropriate procedure and formulas.

After all this laborious and mostly manual steps the result, the longitudinal velocities of the different layers with their respective thickness were presented along each line as geo-seismic sections (Fig. 15, 16, 17 & 18) and as refractor velocity and refractor depth maps (Fig. 13 & 14).

3.3 The electrical resistivity data acquisition, processing and presentation

3.3.1 Instrumentation

The basic equipment required for the electrical resistivity survey consisted of a transmitter, a receiver, electrical cable and electrodes. The instrument used in this survey consists of

Briggs and Stratton 8HP AC motor generator as a power source, Scintrex made *TSQ-3* transmitter as a current control unit and again Scintrex made *IPR-10A* receiver as a potential difference measuring unit. A steel wire is used to connect the two ends of stainless steel current electrodes (A & B) to the transmitter output terminals and the potential electrodes (M & N) to the receiver-input terminals.

3.3.2 The electrical resistivity data acquisition

3.3.2.1 The electrical profiling data acquisition

The electrode arrangement used for profiling was Schlumbereger (Fig. 11b). It was employed for three different depth levels. The half-current electrode separation (AB/2) of 10, 45, and 100 m with their respective half-potential electrode separation (MN/2) 0.5 m, and 6 m (MN/2=6 is used for both AB/2=45 & 100) were utilized. Observation was taken every 20 m interval by moving the whole setup along the profile. In this process 292, 281 and 254 resistivity observations were taken. The actual observations were potential difference *(ΔV)* and current *(I)*, where as the resistivity value is obtained using equation (2.34) by hand calculator. The different number of observations at different levels came from the inaccessibility of moving space. That is why least number of observations are obtained on the AB/2 =100 m level.

3.3.2.2 The electrical sounding (VES) data acquisition

Here again the Schlumberger electrode arrangement (Fig. 11a) is used to perform the VES survey. In this survey observations are made on a fixed VES point by extending the half-current minimum separation 1.5 m to the maximum 220 m (some times 150 m), 5 to 6 measurements within one logarithmic decade. The potential separation will be changed when reading of ΔV approaches zero (weak response). More over the area is covered by 23 VES observations. A minimum of one sounding on three lines and 5 soundings on one profile. There are also lines without VES observations (Fig. 22, 23 & 24).

3.3.3 The electrical resistivity data processing and presentation

3.3.3.1 The resistivity profiling data processing and presentation

The apparent resistivity data obtained at the three depth levels are presented in a map form for each depth levels. The maps are prepared using GEOSOFT mapping system (Geosoft, 1992). From the irregular nature of the survey layout the random gridding with grid cell size of 20 m is used. The grid is contoured and zoned with 5 ohm-m contour interval. Then

the final gridded and contoured map is presented together with the survey layout (Fig. 22, 23 & 24). The latter was made using AutoCAD program (AutoCAD12, 1992).

In addition resistivity-profiling data were plotted as stacked profiles along with the magnetic profile and the geo-electric section and the pseudo section were prepared from VES data for selected profiles (Fig. 25, 26, 27 & 28).

3.3.3.2 The VES data processing and presentation

The VES curves were plotted on bilogarithmic graph papers of modules 62.5 mm, apparent resistivity verses half-current electrode separation (AB/2). The preliminary interpretation was done using partial curve matching technique with two layer master curve and auxiliary point charts. The layer parameters obtained from curve matching were used for final interpretation using computer aided inversion program RESIST.

RESIST is user friendly interactive program (software) for resistivity sounding. The x,y,z data that include AB/2, MN/2 and ρ_{ap} obtained from the field including the initial model parameters obtained by partial curve matching are the inputs for the RESIST. It has an option to fix some model parameters from known sources (geology, well logging, etc.) The program has 30 iterations at the maximum with the default RMS value of 2.5%. It gives as an out put a graphic display of the observed and calculated values and the layer parameters

with their RMS value. Good to excellent sounding curves obtained throughout the area with little or no lateral heterogeneity effects on most of them (Fig. 12).

The final layer parameters were plotted against elevation to construct geo-electric sections (Fig. 25, 26, 27 & 28). The apparent resistivity data was also gridded and contoured to produce pseudo-section using GEOSOFT mapping system (Geosoft, 1992), to see the apparent resistivity distribution along the selected lines.

3.4 The magnetic data processing and interpretation

3.4.1 Instrumentation

The magnetic survey was conducted using Scintrex made *MP-4* magnetometer installed in *IGS-2* (Integrated Geophysical System) console that include *VLF* measuring part. The other parts are the sensor and the backpack harness that is used to fix the sensor on the back of the operator, the sensor cable that connects the sensor to the console and rechargeable battery pack with six rechargeable batteries. *MP-4* measures total field magnetic intensity in a range of 20000 to 100000 gamma with accuracy of ± 2 gamma and resolution of 0.1 gamma.

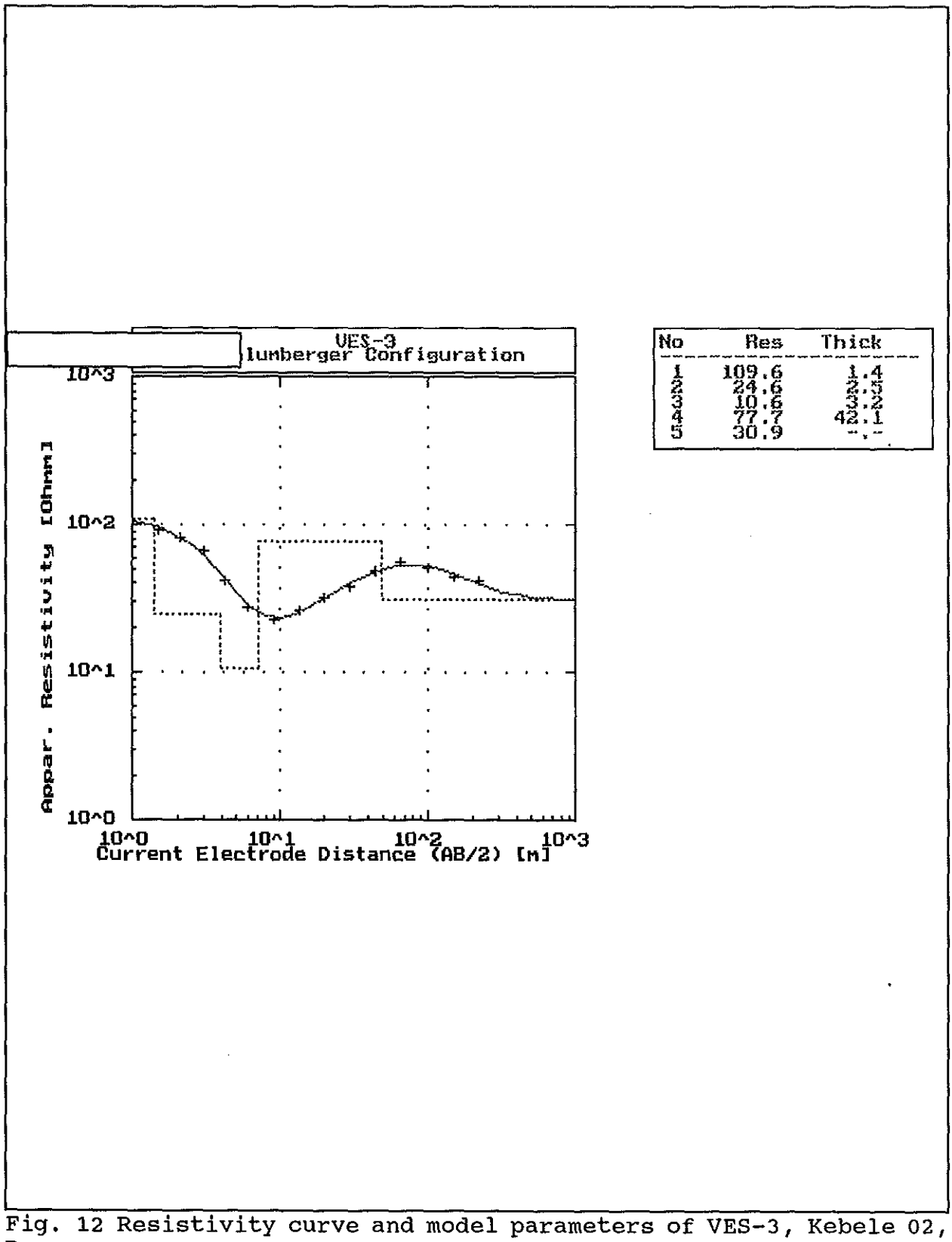

Fig. 12 Resistivity curve and model parameters of VES-3, Kebele 02, Bonga

3.4.2 The magnetic data acquisition

The magnetic data collection is started by establishing a magnetically quiet base station near by the study area. Observations are made every 10 m separation. Each station magnetic reading is accompanied by the respective reading of observation time. Each day's observation is started and completed by taking measurements at chosen base station for subsequent diurnal correction. A total of 579 magnetic intensity readings were made in the area.

3.4.3 The magnetic data processing and presentation

The first step in magnetic data processing was to determine the normal geo-magnetic field of the study area including declination and inclination using the IGRF 4.05.00 GEOSOFT 1995 program that requires as an input the position, time of survey and elevation of the area. The next step was removing irrelevant part of the data using the following diurnal correction formula.

$$B_{corr} = B_i \pm (\Delta B/\Delta t)t_i \pm BT_{\Delta BV} \qquad (3.48)$$

where B_{corr} is corrected total field value, B_i is reading for arbitrary station, ΔB is change in base station value, Δt is change in base station reading time, t_i is reading time for arbitrary

station and $B_{\Delta BV}$ is base value difference (deviation of base value from 34850 nT, which is equivalent to the normal field of the particular area obtained from GEOSOFT program mentioned above).

The corrected total magnetic field intensity data was gridded, smoothed, contoured and plotted using the GEOSOFT mapping system (Geosoft, 1997) with grid cell size 20 m and contour interval 50 gamma (Fig. 19). Applying MAGMAP, one of potential field filtering software of GEOSOFT, vertical first and second derivative filtering were performed. Then the results were presented as first and second derivative maps using the obvious GEOSOFT facilities (Fig. 20 & 21).

CHAPTER 4

RESULT AND INTERPRETATION

4.1 Result and interpretation of the refraction seismic data

4.1.1 Bottom refractor velocity map

The bottom refractor velocity of the area ranges from about 1300 m/s, along line 4, upto 6000 m/s, on the northern high velocity zone (Fig. 13).

According to the velocity distribution, the bottom refractor is grouped into three categories. The first group is with velocity less or equal to 2000 m/s. This zone is mainly situated in the southeastern, eastern central and western central parts of the area. Sporadic lows are also observed in the central parts of the area. These low velocities may be related with rock weathering and fracturing. (Sjogern, 1984). Most of this low velocity zones are in good correlation with the active landslide zones mapped by engineering geology (Fig. 3).

Another velocity category in the area is with refractor velocity greater than 3000 m/s, and it is the response of relatively sound formation with less degree of weathering/fracturing. The

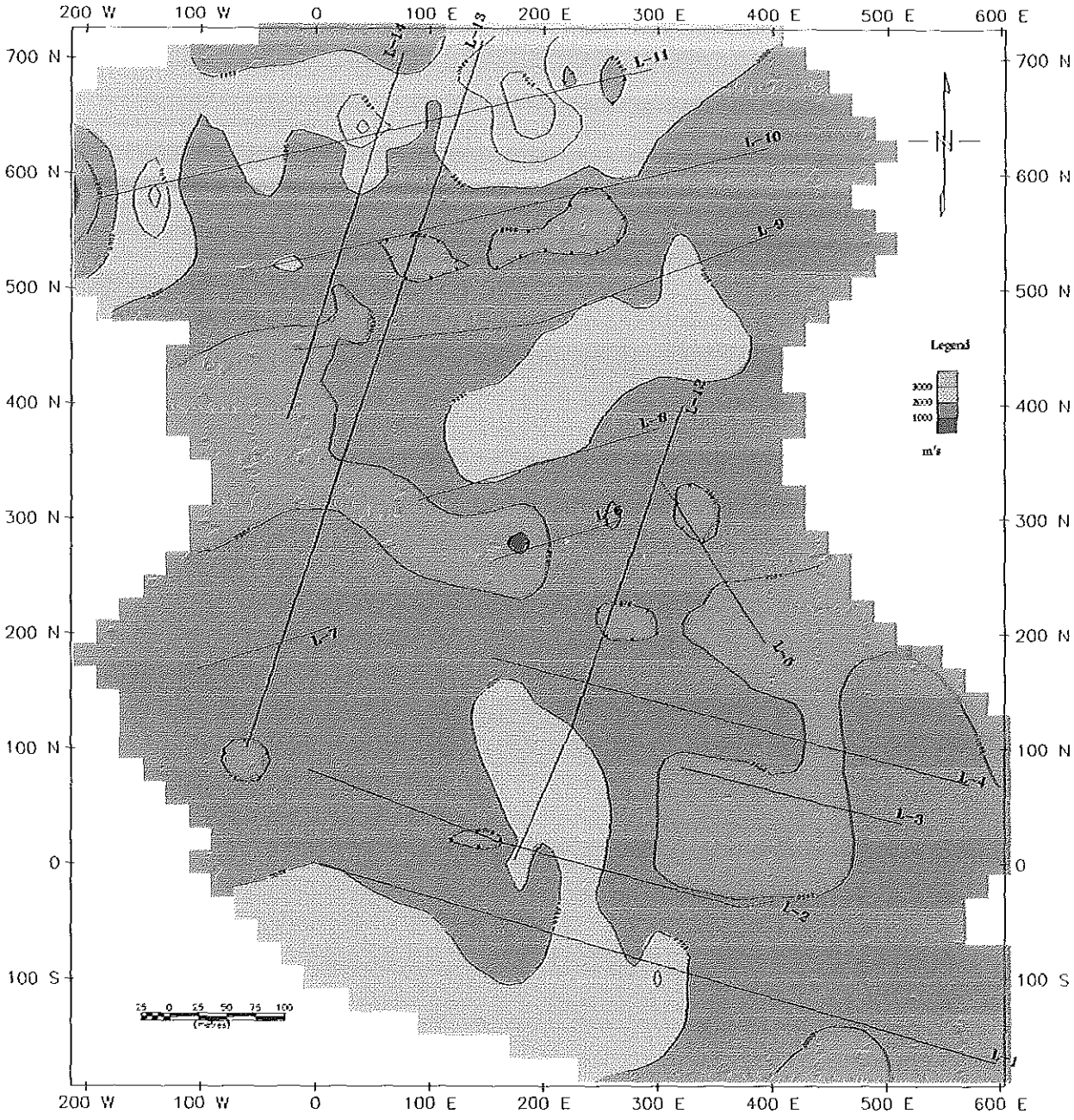

Fig. 13. Bottom refractor velocity map of Kebele 02, Bonga.

Contour intval: 1000m/s

northern part that covers most part of line 11, the area between lines 8 & 9, and the central southern part that touches lines 1, 2 & 12 lies in this group.

The intermediate refractor velocity, between 2000 & 3000 m/s, forms the third category that covers the rest of the survey area. The direct correlation between rock quality and velocity favor this area as easily susceptible zone for any landslide phenomena next to the low velocity zone.

4.1.2 Depth to the bottom refractor map

One of the outputs of seismic refraction survey is the determination of depth to the bottom refractor (Fig. 14). Mostly lower velocities correspond to shallower depths while the higher velocities are associated with deep-seated formations. The least bottom refractor velocity zone between line 9 & 10, the central parts around line 6 & 8 and the western half of line 3 correspond to the shallower zone with 5-10 m depth. The maximum refractor depth (32 m) is found within the southern central deeper zone. It exhibits more than 3000 m/s velocity as shown on the velocity map (Fig. 13).

The intermediate velocity zone (2000-3000 m/s) that covers the larger portion of the study area is found between 10 and 15 m depth. The northern high velocity zone mostly lies in the range of 15-20 m.

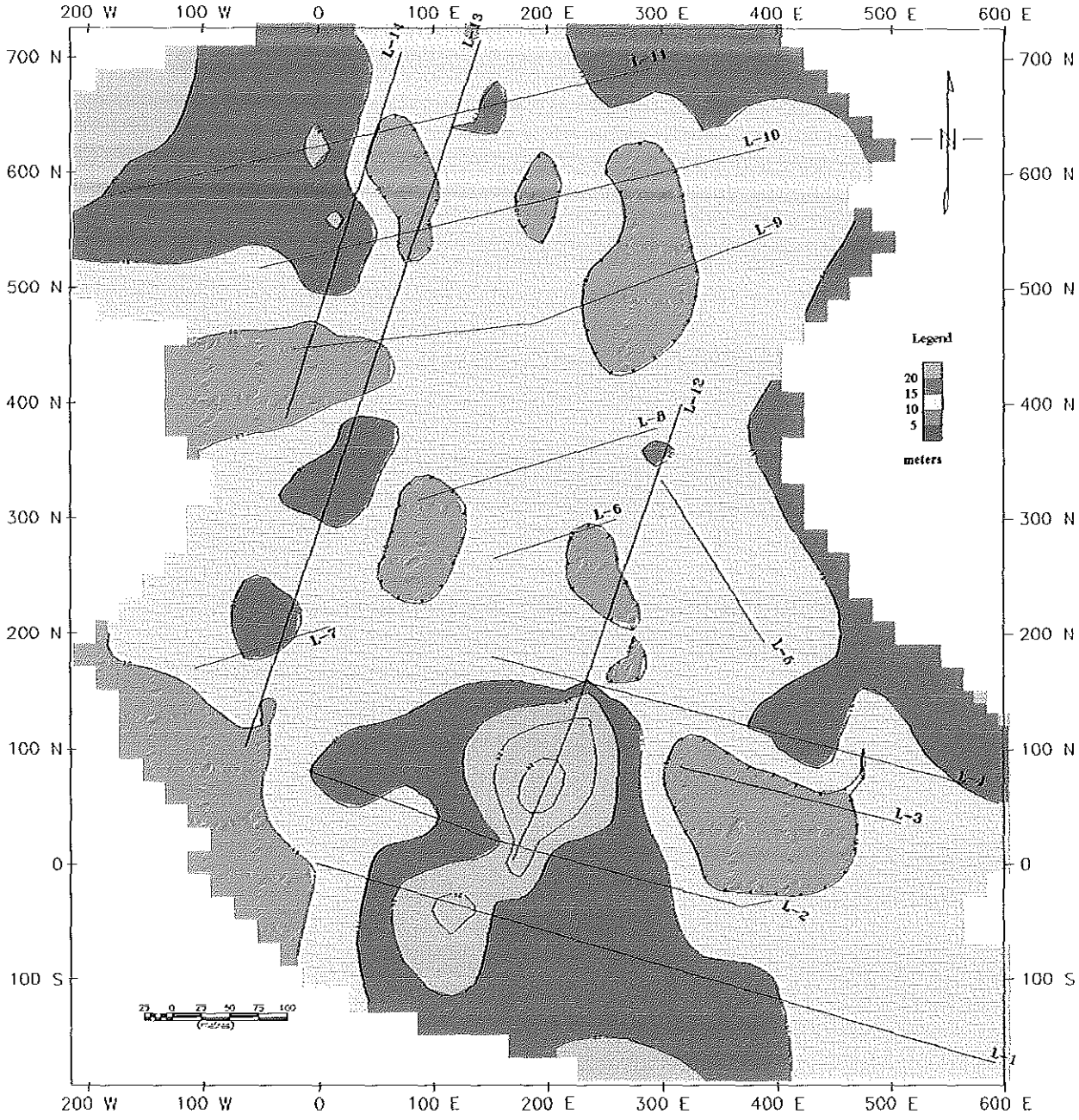

Fig. 14. Depth to the bottom refractor map of Kebele 02, Bonga.

Contour intval 5m

4.1.3 Result and interpretation of the refraction seismic section

From all fourteen surveyed lines with shallow seismic refraction method (to avoid redundancy) only four profiles (as in the case of electrical) are selected for detail discussion. These four profiles are believed to be highly representative area-wise and more informative.

Line-1

Seismic section along line-1 (Fig. 15) exhibits three velocity layers (two seismic wave refracting boundaries).

The top relatively low velocity layer comprises longitudinal velocities ranging from 330 m/s at the extreme east of the profile to 825 m/s around location 250 m. Both the seismic result and my field observation show disagreement with the geology (Fig. 3) of the area (west of 300 m location along line-1) which is described as basalt, whereas the seismic velocity obtained is very low to that of expected from weathered basalt. The first refractor surface doesn't show any significant undulation. It is almost an image of the topography with an average thickness of 5.5 m with an exception of 3 m thickness around 330 m location and the extreme east of the line.

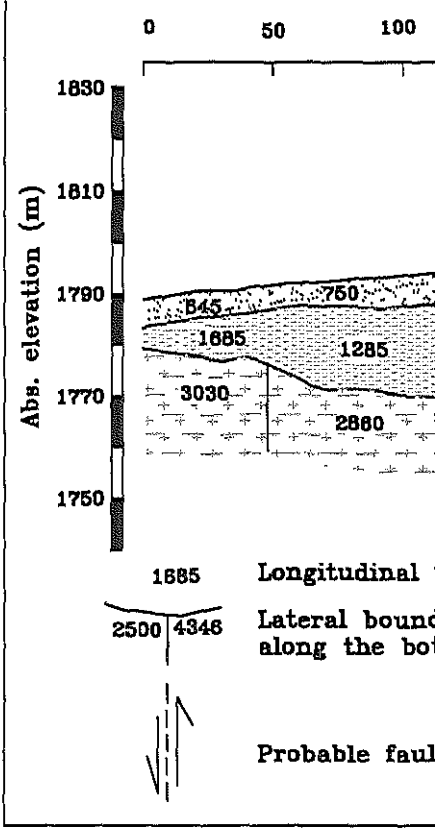
0
50
100
1830
1810
1790
1770
1750
Abs. elevation (m)
845
750
1685
1285
3030
2880
1685
Longitudinal
2500
4346
Lateral bound
along the bo
Probable faul

Fig. 15 Se

The second intermediate velocity layer exhibits a maximum velocity of (1685 m/s) in the eastern margin (around 15 m) and a minimum velocity of 900 m/s about location 500 m. The thickness of this layer attains the maximum thickness (18 m) around location 130 m, and it becomes thinner (6m) around 500 m location. The second refractor (which is the bottom refractor) shows a depression between 70 m and 150 m locations, where the maximum thickness of the second layer is observed, and it extends up to profile 4 along line 12. The thickness of this layer becomes small around location 180 m and again an increase is observed towards 350 m location. From this position on ward layer thickness becomes thinner and almost follows the morphology of the topography.

The velocity along the bottom refractor shows frequent lateral variations within the range of 2020-4346 m/s that is typical in most of the survey area. The parallel displacement on the residual time distance curve at 475 m and 260 m location is interpreted as structure, possibly a fault.

Except the landslide scarp around 475 m, this profile is free of any landslide indications. The relatively higher velocity of the top layer signifies that the colluvial soil in the area is relatively consolidated than the surrounding rock masses.

Line-4

The seismic section along line 4 (Fig. 16) reveals that the top most relatively uniform velocity (290-440 m/s) layer has about 3m thickness. Similarly to that of line-1, the velocity of the top surface at the ends of the profile is too low to correlate as the response of basalt as indicated on the geology map (Fig. 3). The least velocity 290 m/s is obtained around location 60 m, where the possible structure is inferred to be associated with surface landslide manifestations.

The underlying velocity layer acquires the maximum velocity (1640 m/s) about location 180 m and the minimum (740 m/s) between locations 60 m and 130 m indicating that the land slide phenomena observed at the surface is also continuous at depth. The thickness of this layer varies from place to place with its minimum (6m) at location 90m and maximum (16 m) at location 280 m. From 350 m onwards the layer undulates following the topography and has a uniform thickness of about 12 m.

The velocity of the substratum (the third layer) is generally low, in particular a velocity of 1250 m/s, 2000 m/s, and 1430 m/s are obtained between locations 40 m - 65 m, 210m - 250 m, and 275 m - 310 m respectively. A 2000 m/s longitudinal velocity is also observed at the eastern part of the line. These low velocities are attributed to highly fractured and weathered week zones crossing the line which is clearly manifested by cracking and active landslide scarp on the geology of the area (Fig. 3). The rest part of the bottom layer range

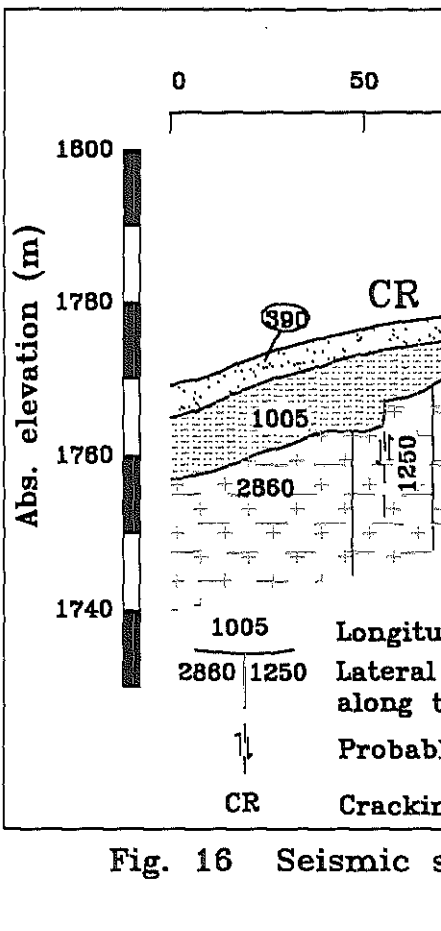

Fig. 16 Seismic s

between 2174 m/s and 2860 m/s velocity which could be associated with the character of rocks where the weathering effect become minimal.

Line-10

The velocity distribution of the top layer, along line 10 (Fig. 17), is very low. It is in the range of 234 - 340 m/s except at the extreme east of the profile, where 410m/s velocity is encountered. This low velocity is most probably due to the response of the top dry loose soil with some active landslide indications. The thickness of this velocity layer varies from 7 m at the western end of the profile to zero at about location 150 m (where the western stream crosses the profile). The central part of the profile that is bounded by the two streams (i.e between locations 170 m and 380 m) retains 1 to 4 m thickness, whereas along the eastern up-sloping topography it varies from 2 to 7 m.

The middle seismic layer overlying the bottom refractor has a velocity range 1000 - 1440 m/s except the area around location 350 m that is characterized by a velocity of 675 m/s. This seismic layer has a 5 m thickness at about locations 40 m, 290 m and 350 m, and increases to about 11 m between locations 150 m and 200 m along the profile.

The velocity of the bottom refractor varies from medium to low. Least of all 1400 m/s and 1375 m/s were obtained at around 160 m location (underlying the western stream) and at 325 m respectively. These low velocity zones having upto 20 m width are the possible

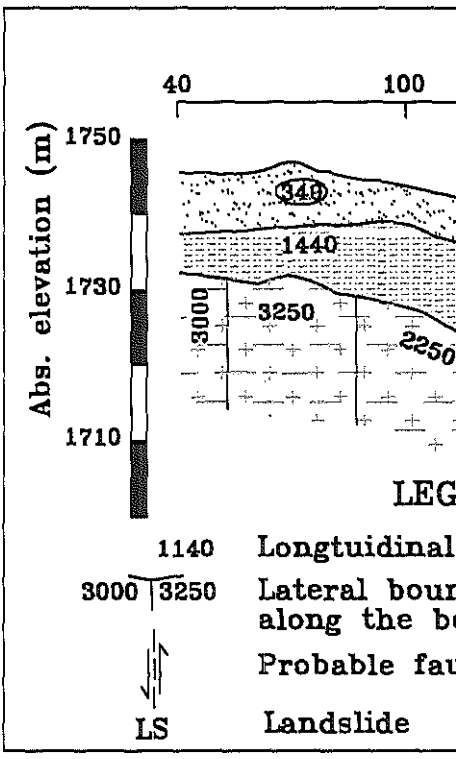

Fig. 17 Seismi

weak zones, which have good association to surface landslide indications (Fig. 3). The western part of the profile west of 80 m has the maximum velocity 3250 m/s. The rest of the substratum is represented by 2000 m/s - 2350 m/s velocity, which is the response of weathered/fractured formations.

Line-13

As in the cases of previous profiles, on this nearly N-S oriented line, the seismic section (Fig. 17) shows low velocity (215 - 420 m/s) for the top layer. A 45 m/s short interval velocity zone, corresponding to the landslide scarp crossing the line interrupts a longitudinal velocity of 365 m/s, which is shown at the relatively elevated southern part of the profile. Further to the south it is followed by a 420 m/s velocity layer, covering the wide down sloping central part except the thin layer (about 1m thick) with a velocity of 315 m/s around 300 m location. The right and left banks of the western stream that cross the line at 470 m are marked by the least top layer velocity (215 m/s) that could be accompanied with active landslide conditions in the area. Adjacent to it, there is a steep slope portion with a relatively higher top layer velocity that reaches 375 m/s, at the extreme end of the line beneath the 600 m location. The thickness of this layer varies from 3 to 5 m, from the southern end of the profile up to 350 m location. This top velocity layer at the northern end of the profile has 2-3 m thickness.

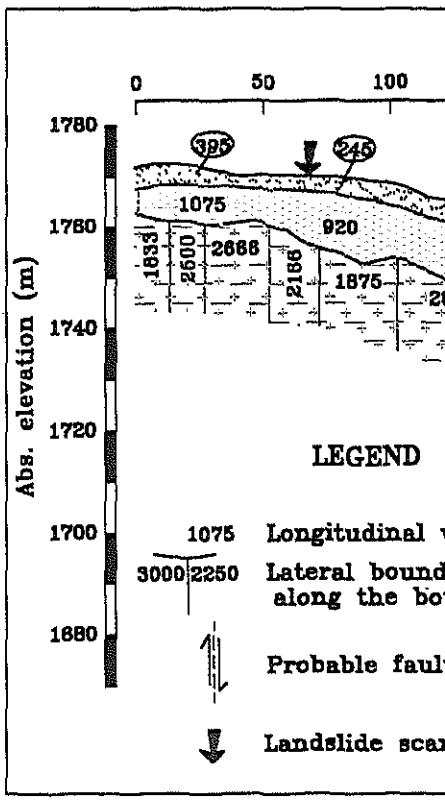

Fig. 18 Seismic se

The underlying velocity layer (2nd layer) shows similar trend of velocity distribution as that of the overlying layer, the only difference being a change in magnitude. For example, the maximum 1535 m/s velocity is observed beneath the 420 m/s, relatively higher top layer velocity. Similarly the minimum 390 m/s velocity layer beneath the stream at 470 m location is in agreement with the least top layer velocity (215 m/s). This correspondence indicates that the surfacial unstable condition (probably the loose colluvial formations favoring landslide occurrences) observed along the profile is also continues depth wise.

The thickness of this middle layer varies from 4m at the location of the stream (470 m) upto 12.5 m around 220 m location. Generally the thickness of the 2nd layer shows a south-north increase despite local thinning observed from 310 m upto 320 m location and around the vicinity of the stream.

The velocity of the bottom refractor is generally erratic and lateral velocity change is observed within short gap on an average of 30m interval. The first 10m interval in the south and the intervals between locations 70 m - 150 m, 210 m - 270 m, 310 m- 325 m and 375 m - 400 m are grouped as the least velocity zones (shear zones), with velocities less than or equal to 2000 m/s. The area north of 500 m is characterized by relatively higher velocities (> 3000m/s), without any landslide indication. The maximum bottom refractor velocity (6000 m/s), is observed beneath 370 m. Furthermore, this seismic survey has indicated occurrences of probable faults at about locations 170 m, 370 m and 540 m along the profile.

4.2 Result and interpretation of the magnetic data

4.2.1 Total magnetic field map

Figure 19 shows the total field magnetic intensity map of the study area compiled using the 579 observations. The map indicates the total magnetic field variations ranging (from 34500-35200 nT) in the study area. The trend and orientation of the iso-magnetic contours is generally NNW-SSE that is consistent with the trend of geological structures confirmed by the engineering geological map (Fig. 3) and the field observations. The distributions of the total field magnetic values displayed by the map (Fig. 19) is alternating bands of highs and lows (high, low, high and then low) when going from west to east. There also exist localised pockets of highs and lows whose shapes vary from a nearly circular to elliptical. This highs and lows are thought to be associated with the relative susceptibility of the geologic units mainly varying grades of basalts, colluvial deposits and intercalation of both that constitute the study area (Fig. 3). Accordingly the relatively higher values trending in the NNE direction on the western and central parts are associated with fresh to moderately weathered, very closely jointed and medium to strong basalt of relatively higher susceptibility. The corresponding lows with a trend identical, as those of the highs (NNE-SSW) are associated with the colluvial deposits of relatively lower susceptibility than the basalts. An approximately E-W oriented magnetic low bisects the NNW-SSE oriented magnetic high zone in the central part. This E-W oriented magnetic low is thought to be the

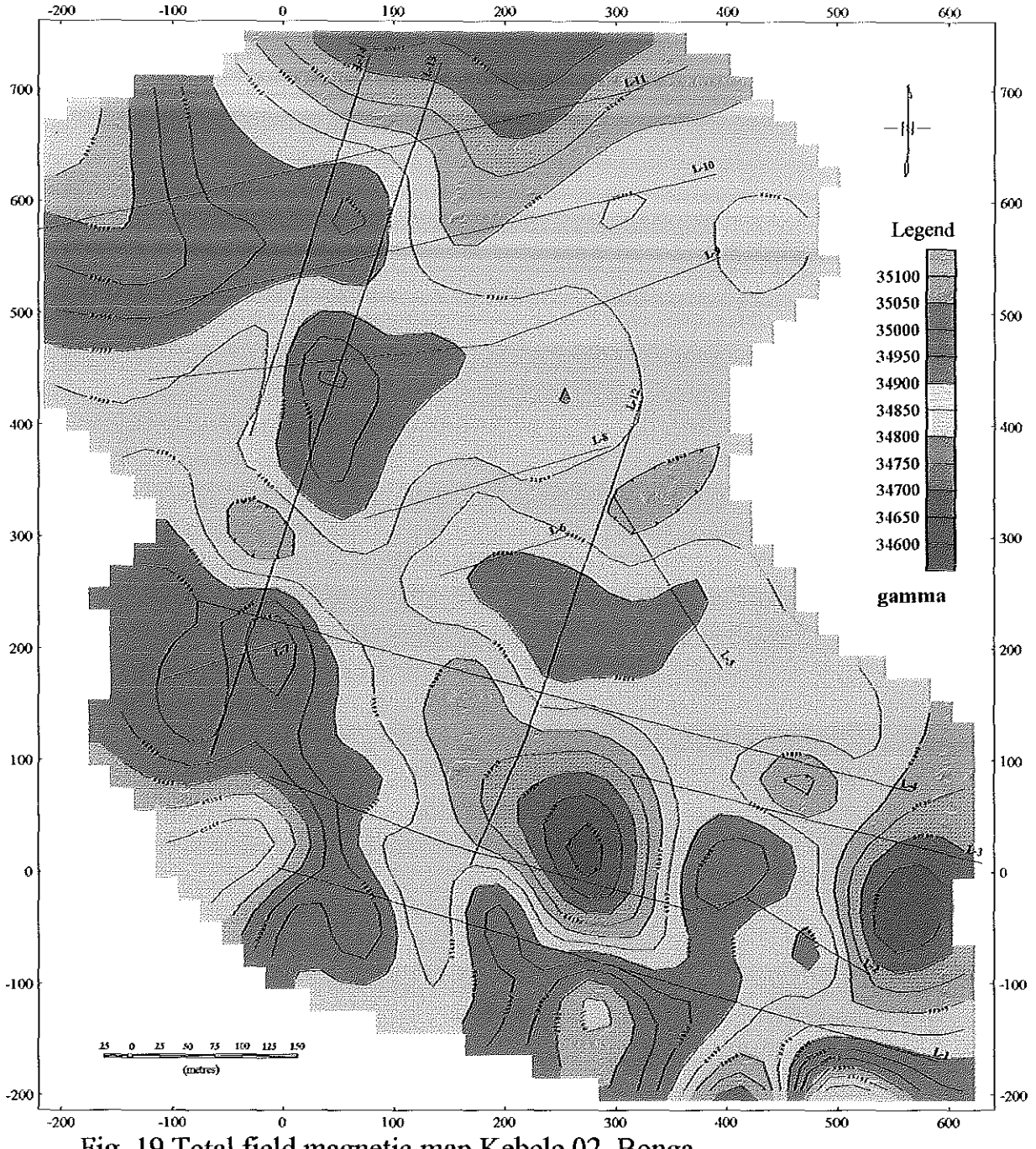

Fig. 19 Total field magnetic map Kebele 02, Bonga

Contour interval: 50gamma

response of colluvial deposits masking (overwhelming) the NNW-SSE oriented high magnetic response of the basaltic materials. The likely occurrence of a large volume of colluvial deposits along the E-W oriented low magnetic response is can be thought to be favoured by the landslide scarps shown on the geology map and frequent landslide occurrences from the landslide history of the area and the conducive topographic gradient favouring this phenomena along the E-W oriented low magnetic zone. The same E-W oriented magnetic low is observed along the orientation of line 10 and at the extreme southeastern part of the area.

4.2.2 Vertical derivative maps

The derivative maps acts as a filter, emphasises the expressions of local features, and removes the effects of large anomalies or regional influences (Nettleton, 1976). The NNW-SSE trending relatively high and low magnetic responses that are observed on the total field magnetic map (Fig. 19) were enhanced on the first derivative map (Fig. 20). The nearly E-W trending low magnetic trends that interfere the NNW-SSE alternating highs and lows are clearly delineated by the negative one contour line. The northeastern relatively quiet magnetic response on the total field map (Fig. 19) also enhanced by the first derivative maps. The major landslide scarps shown on the engineering geology map (Fig. 3) were outlined by the zero contours on the second derivative map (Fig. 21). They are interpreted as probable faults indicated by heavy broken lines F1F1', F2F2', F3F3' and F4F4' (Fig. 21). The E-W trending

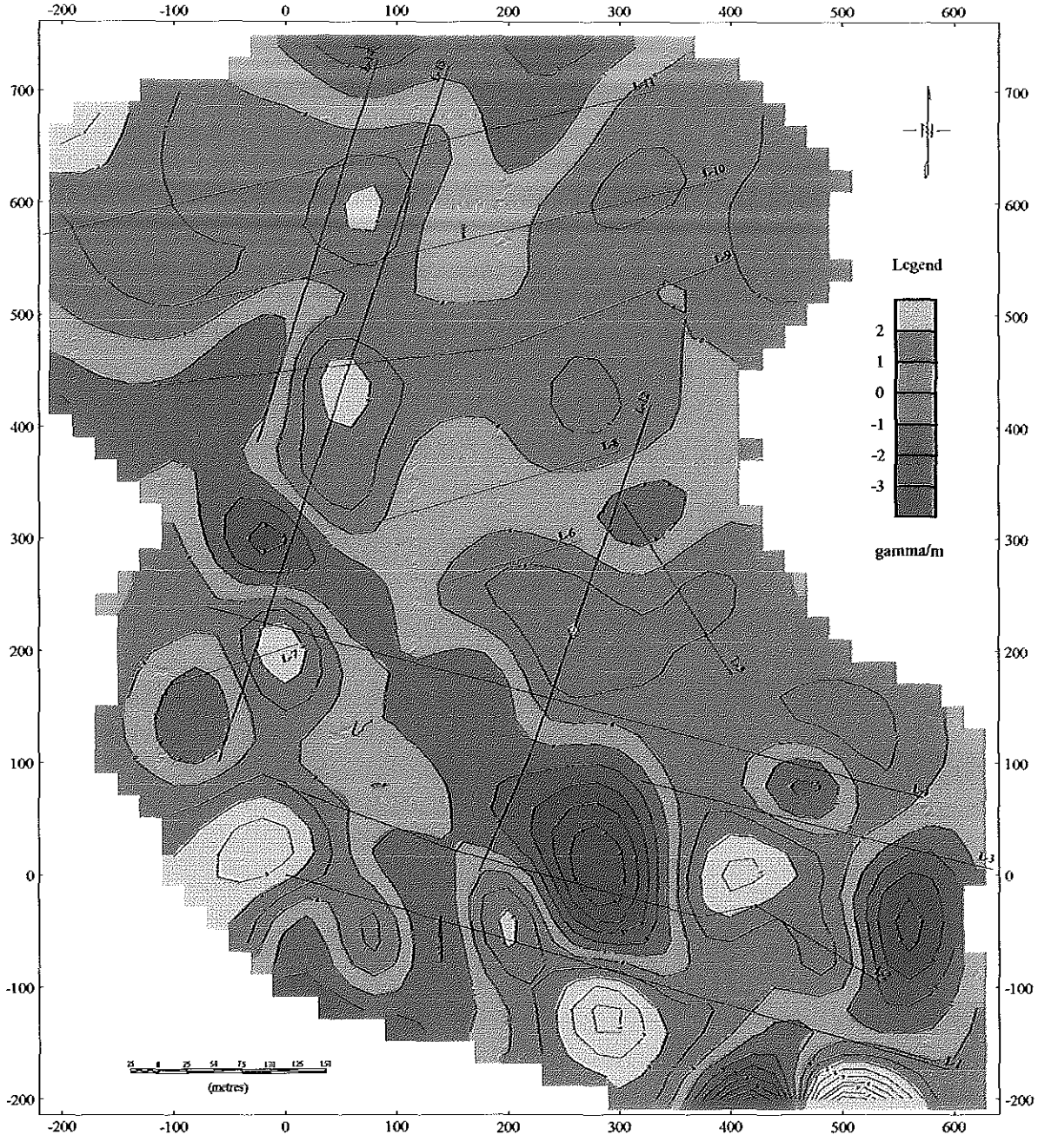

Fig. 20 Vertical first derivative total field magnetic map of Kebele 02, BONGA.

weak zone faintly observed along the orientation of line-10 on the total field map (Fig. 19) is clearly demarcated by the zero contour on the second derivative map, which is associated with some landslide indication on the engineering geology map (Fig.3).

The NNE-SSW trending fault (F1-F1'), that crosses the eastern part of profiles 1,2 & 3, is characterised by high magnetic gradient which corresponds with a low velocity zone (i.e. below 2200 m/s). This structural feature separates the eastern basaltic zone from the western landslide affected colluvial soil covered area (Z-5).

The F2-F2' probable fault with the same trend as that of F1-F1' found between lines 10 & 11 delineate the northern relatively stable zone from the highly active landslide zone (Z-5). High magnetic and high resistivity gradient and low refractor velocity (less than 2000 m/s) characterise this inferred structure.

The NNW-SSE trending probable fault (F3-F3') is aligned with the landslide scarp that affects many of the administration offices. It is delineated by high magnetic and electrical gradient with low refractor velocity (less than 2500 m/s).

The other inferred fault (i.e. F4-F4'), along the eastern landslide scarp that coincides with the perennial stream and its bank covered by alluvial soil. This feature delineates the eastern relatively stable residual soil covered part from the western landslide zone.

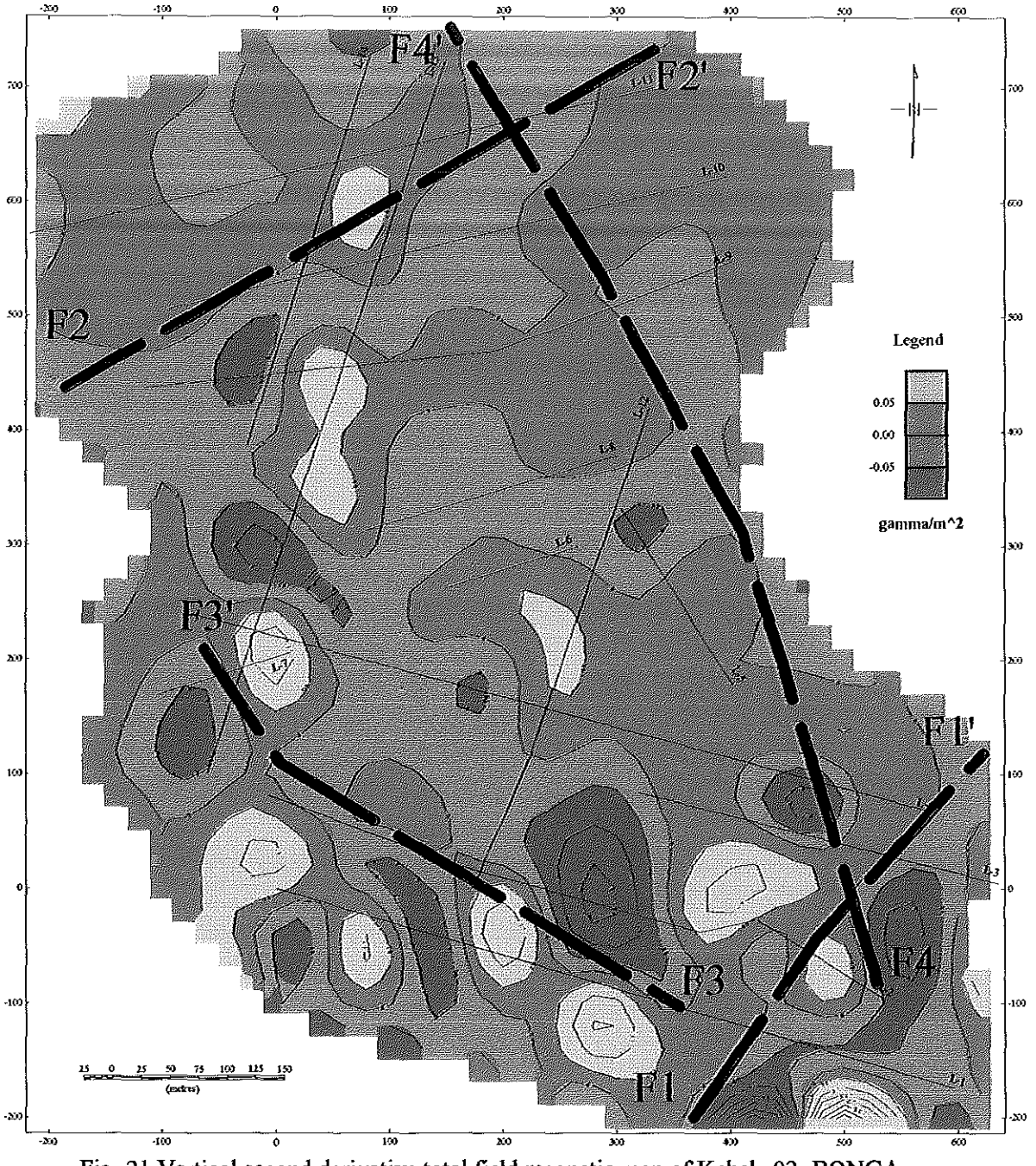

Fig. 21 Vertical second derivative total field magnetic map of Kebele 02, BONGA.

An important point that worth mentioning here is a good correlation of the magnetic maps (Fig. 19, 20 & 21) with that of resistivity map at the level of AB/2=10 m (Fig. 22). This similarity of frequently varying electrical and magnetic trends are assumed to be due to the heterogeneity of soil and rock masses involved in the near surface of the area that is highly affected by the landslide phenomena.

4.3 Result and interpretation of the electrical resistivity data

4.3.1 Resistivity maps

The lateral apparent resistivity distribution of the survey area is illustrated in three maps (Fig. 22, 23 & 24) corresponding to three levels of AB/2=10, 45 and 100 m.

The map, at the level of AB/2=10 (Fig. 18), that shows the response from about the depths, 4 - 7 meters is characterized by relatively higher resistivity values at the extreme SW, SE, NW, and NE ends of the survey area. While the rest parts of the map are marked by relatively medium to low resistivity responses of the same depth range 4 - 7 m. The high resistivity values at the SE and SW corners might be correlated with the varying grades of basalts mapped by the engineering geology (Fig. 3). The highs at the NW and NE are might be due to any relatively hard volcanic rock most probably basalt underneath the colluvial soil. The remaining medium to low resistivity values might be due to the moisture content and degree of cementation of the colluvial soil covering most of the central parts of the area (Fig. 22).

The resistivity distribution at the AB/2=45 m (Fig. 23), shows a general trend extending from NNE to SSW. The relatively lower and wider resistivity zone (< 25 ohm-m) that extends from NNE - SSW along the central part of the area is engulfed by relatively higher (> 25 ohm-m) resistivity zones along its northern, western and southeastern flanks. The

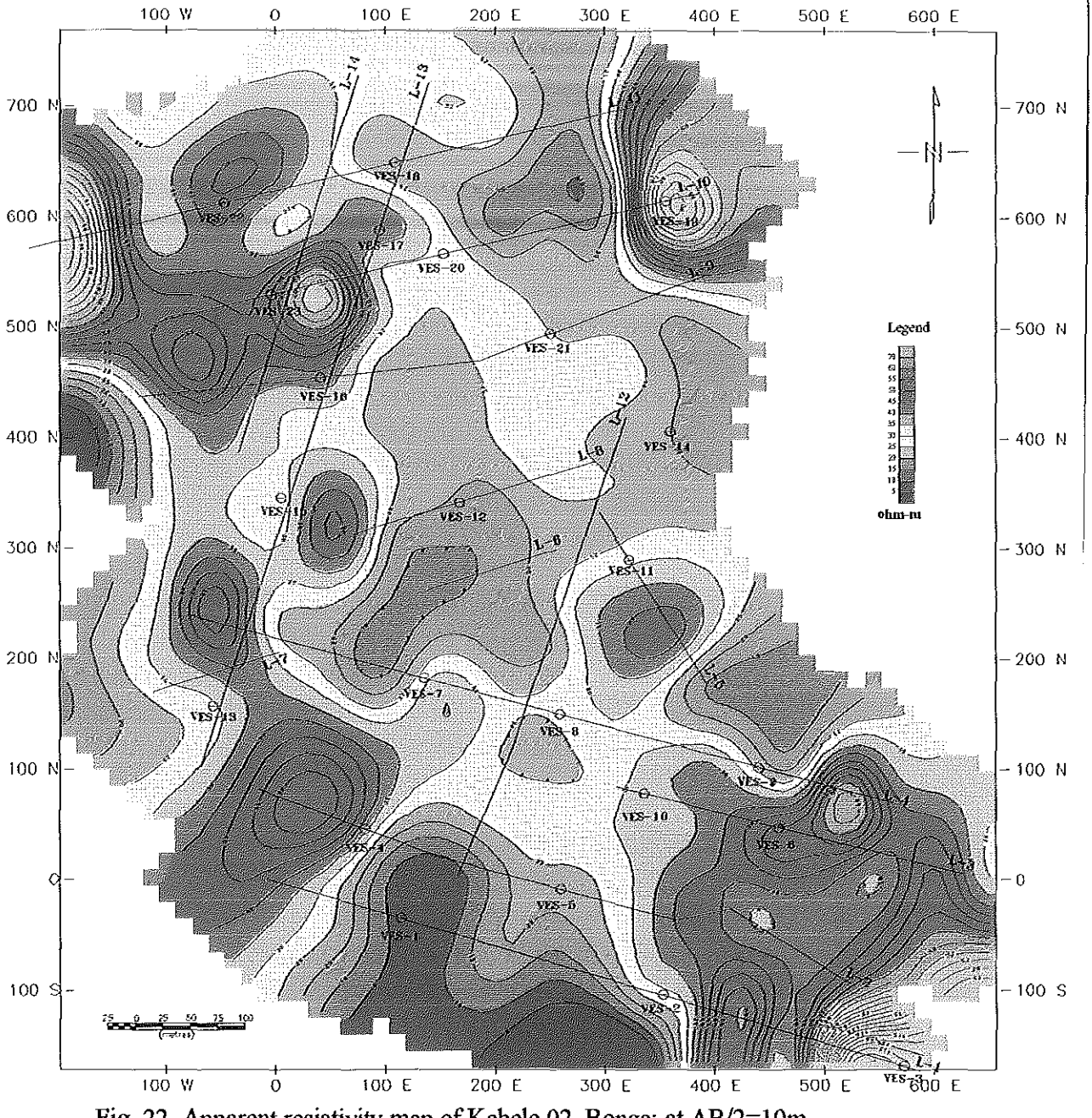

Fig. 22. Apparent resistivity map of Kebele 02, Bonga; at AB/2=10m.

Contour interval: 5ohm-m

resistivity range in the central part of the AB/2=10 m level was 5 – 60 ohm-m where as here is 5 – 35 ohm-m only. This effect of contrast seems to reflect an increase in the degree of water saturation downwards, where this increase in water saturation in turn decreases the resistivity values of the rock masses involved. The important characteristics reveled by both maps (Fig. 22 & 23) that there seems to be a general decreasing tendency in resistivity values with depth.

The third level, AB/2=100, which has a potential to reach about 40 m depth (Fig. 24), in comparison to the previous levels (AB/2=10 m & AB/2=45 m). The resistivity distribution for this level (Fig. 24), reveals a nearly similar pattern and trend to that of level AB/2=45 m (Fig. 23) in comparison to that of level AB/2=10 m. This similarity in resistivity distribution signifies that there is a general decrease in heterogeneity of rocks with depth, for example the heterogeneity in rock masses for level AB/2=100 m is less than that of AB/2=45 m. On the other hand, the formation compactness that associates with the decrease in degree of weathering and jointing is in agreement to the rate of variation of resistivity values for the three-depth levels considered.

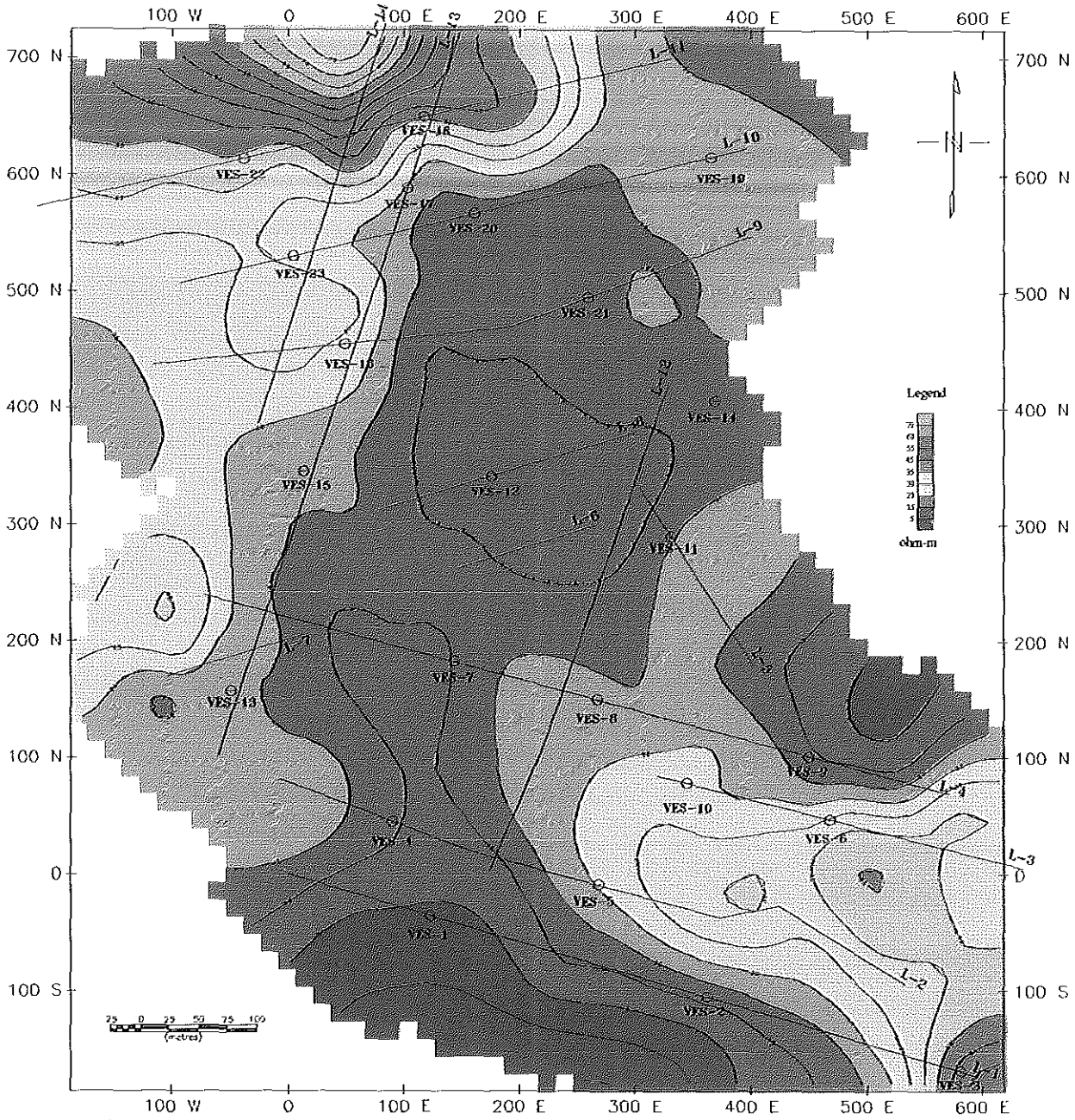

Fig. 23. Apparent resistivity map of Kebele 02, Bonga; at AB/2=45m.

Contour intval: 5ohm-m

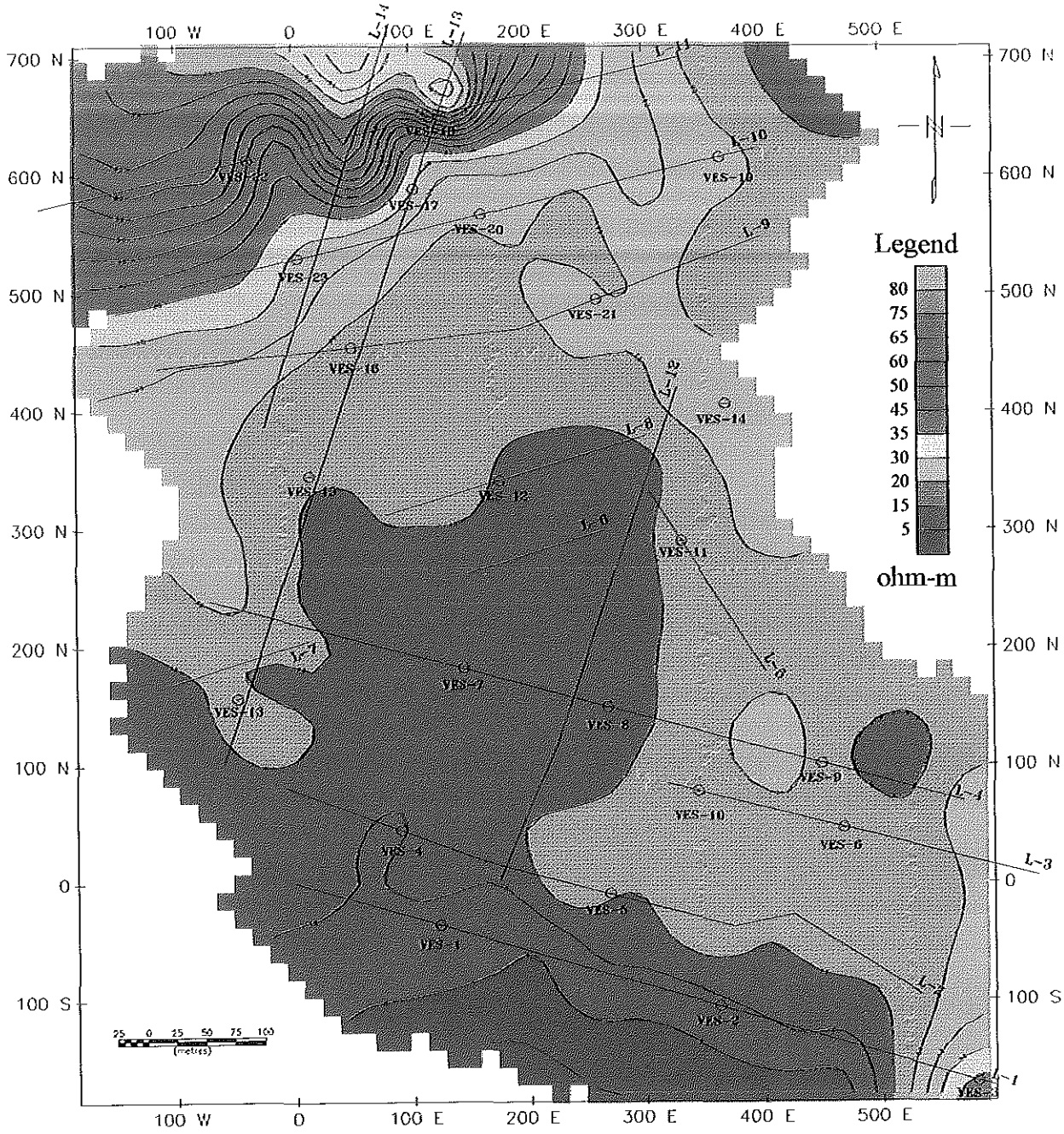

Fig. 24. Apparent resistivity map of Kebele 02, Bonga; at AB=100m.

Contour interval: 5ohm-m

4.3.2 Electrical resistivity sections

On the selected survey lines, particularly, lines 1, 4, 10 and 13, where sufficient soundings exist (at least >2), apparent resistivity pseudo-section, geo-electrical section and electrical profiling plots for the three levels (AB/2=10, 45, & 100 m) are plotted as shown by figures 25, 26, 27 and 28. These plots (Fig. 25, 26, 27 & 28) also include a plot of the magnetic profiles of the total field magnetic data observed along the lines considered (i.e. 1, 4, 10, & 13)

Line 1

The apparent resistivity pseudo section along line 1 (Fig. 25b) shows that there are alternating resistivity layers which vary as high, low, and then high, resistivity values corresponding to the decrease in heterogeneity of rock formation, water saturation and degree of weathering with depth. This alternating variation in resistivity values is also laterally observed on all the apparent resistivity maps (Fig. 22, 23 & 24) compiled for the three depth levels (AB/2=10, 45, & 100 m) considered along the orientation (EW) of the selected lines.

According to the geo-electrical section (Fig. 25c) five geo-electric layers are constructed along the line. The top layer has resistivities ranging from 39 ohm-m to 110 ohm-m and

generally increasing from west to east along the profile with approximately a uniform thickness of 1.3 m.

The second geo-electric layer, unlike the top layer, shows a decrease in resistivity values from west to east ranging from 25 to 95 ohm-m. A maximum thickness 4.5 m of this layer is attained at about the location of VES-2. There is also a general decrease in thickness of this layer both to the left and the right of VES - 2, the minimum is reaching upto 0.6 m west of VES - 2 beneath VES - 1.

The third geo-electric layer shows significant variations both in resistivity values and thicknesses. These variations are also manifested on the apparent resistivity pseudo-section (Fig. 25b) at about 500 m location with the deflection of the resistivity isolines to the left and right about this location (500 m). Comparison of the plots for electrical profiling at the three depth levels and the magnetic data along the line at about the same location (500 m) in Fig. 25a, a sharp increase in resistivity and a disturbance in the magnetic response is apparent. The occurrence of these resistivity and magnetic phenomena may be ascribed to be due to a structure in vertical contact (probably the fault that is marked as an active landslide scarp) on the geology map (Fig. 3).

The next least resistive, 5-7 ohm-m fourth layer to the left of the 500 m location extends to a maximum thickness of about 102 m at about 460 m location. This low resistivity is due to less weathered, highly fractured and highly water saturated formations (most probably basalt).

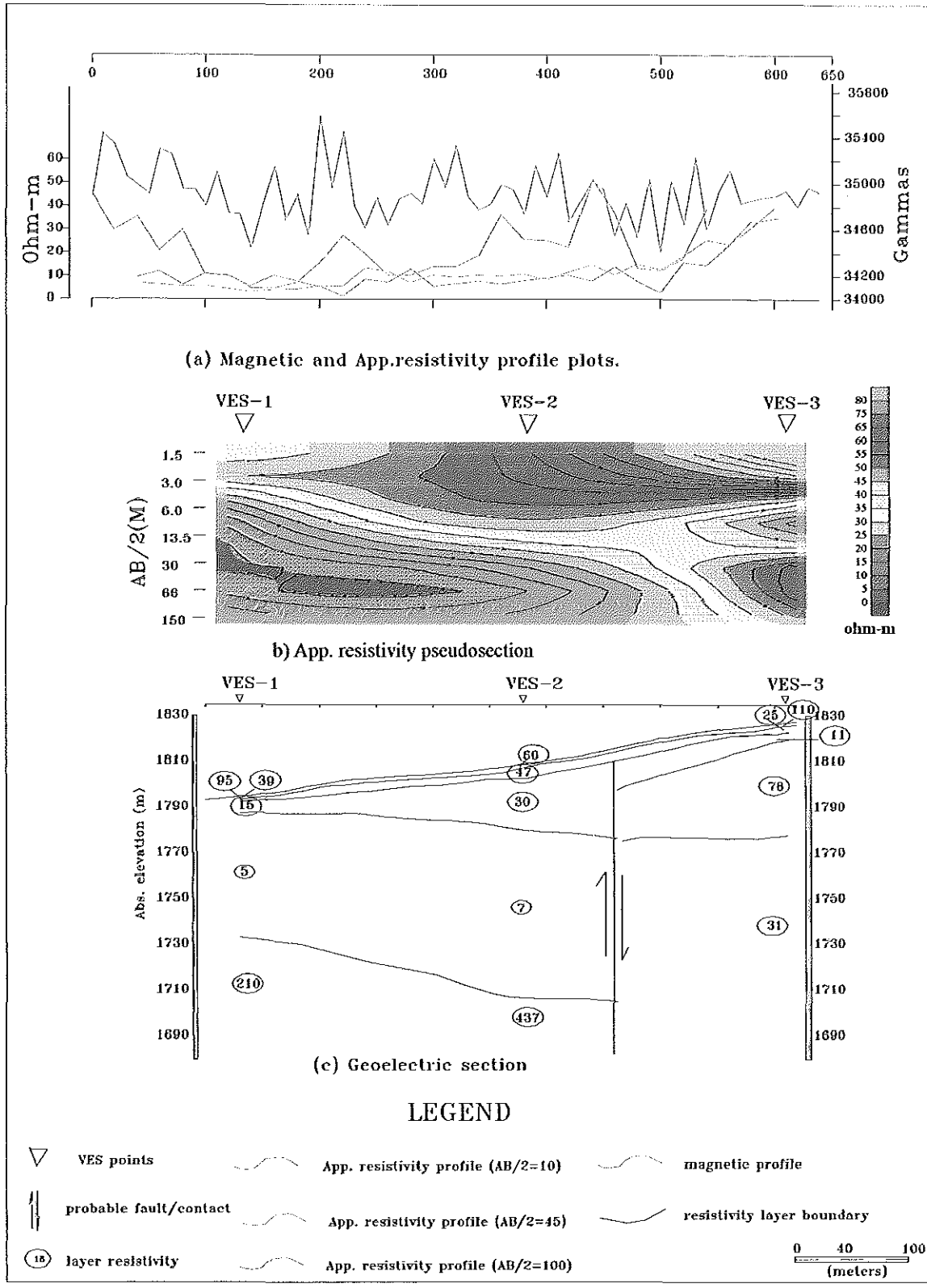

Fig. 25. Results of electrical and magnetic surveys along line-1, Kebele 02, Bonga.

The fourth layer to the right of the 500 m location is registered with 78 ohm-m resistivity and 42 m thickness.

The last and bottom layer to the left of 500 m location obtained, by the maximum current electrode spacing, is a relatively resistive layer (less weathered to fresh volcanic rocks) with resistivity values ranging between 210 and 457 ohm-m. While to the right of the discontinuity at the 500 m of location it attains a value of 31 ohm-m only starting at a relatively shallow depth (50 m from surface).

Line-4

The pseudo-section along profile-4 covers only the central part (between -10 m to 300 m) of the line (Fig. 26b). The resistivity distribution shows high at the extreme ends of the pseudo-section that decrease toward its center. Moreover, this decrease in resistivity is also evident to occur depth wise at the extreme ends of the pseudo-section.

From the geo-electric section (Fig. 26c), 5 to 6 resistivity layers are outlined. The resistivity of the top most layer varies from point to point; along the line where its central part extending from 50 m to 500 m location, exhibits the least resistivity 18 ohm-m with a maximum of 1.5 m thickness. The top layer on western flank part shows a maximum resistivity of 84 ohm-m and thickness of 1.8 m. The western flank and the central part are dissected by a shallow vertical feature (a fracture or shallow fault) that extend up to the 4th

geo-electric layer that correspond to the western flank and the 5th layer of the central part from the surface at the location of 50 m. The existence of this feature is also clearly evident on the seismic section (Fig. 16) and on a magnetic plot (Fig. 26a).

The third geo-electric layer is less resistive than the upper layer with 11-19 ohm-m resistivity values and 5 - 7 m corresponding thicknesses. There is a localized relatively resistive geo-electric layer with resistivity 58 ohm-m bounded by the assumed fault at about 50 m location to the west and that pinches out at about 260 m location.

The underlying low resistive geo-electric layer extends beneath all along the profile with resistivity range of 5 - 10 ohm-m and maximum thickness of 38 m near station zero which decreases to 24 m about location 300 m. The low resistivity response that might be due to highly fractured and water saturated basaltic material which allow circulation of water through it.

The deepest layer along this profile is characterized by relatively higher (25 - 42 ohm-m) resistivity value. This relatively higher resistivity value is thought to be the response of a basaltic material that has low water saturation and whose degree of weathering is relatively low.

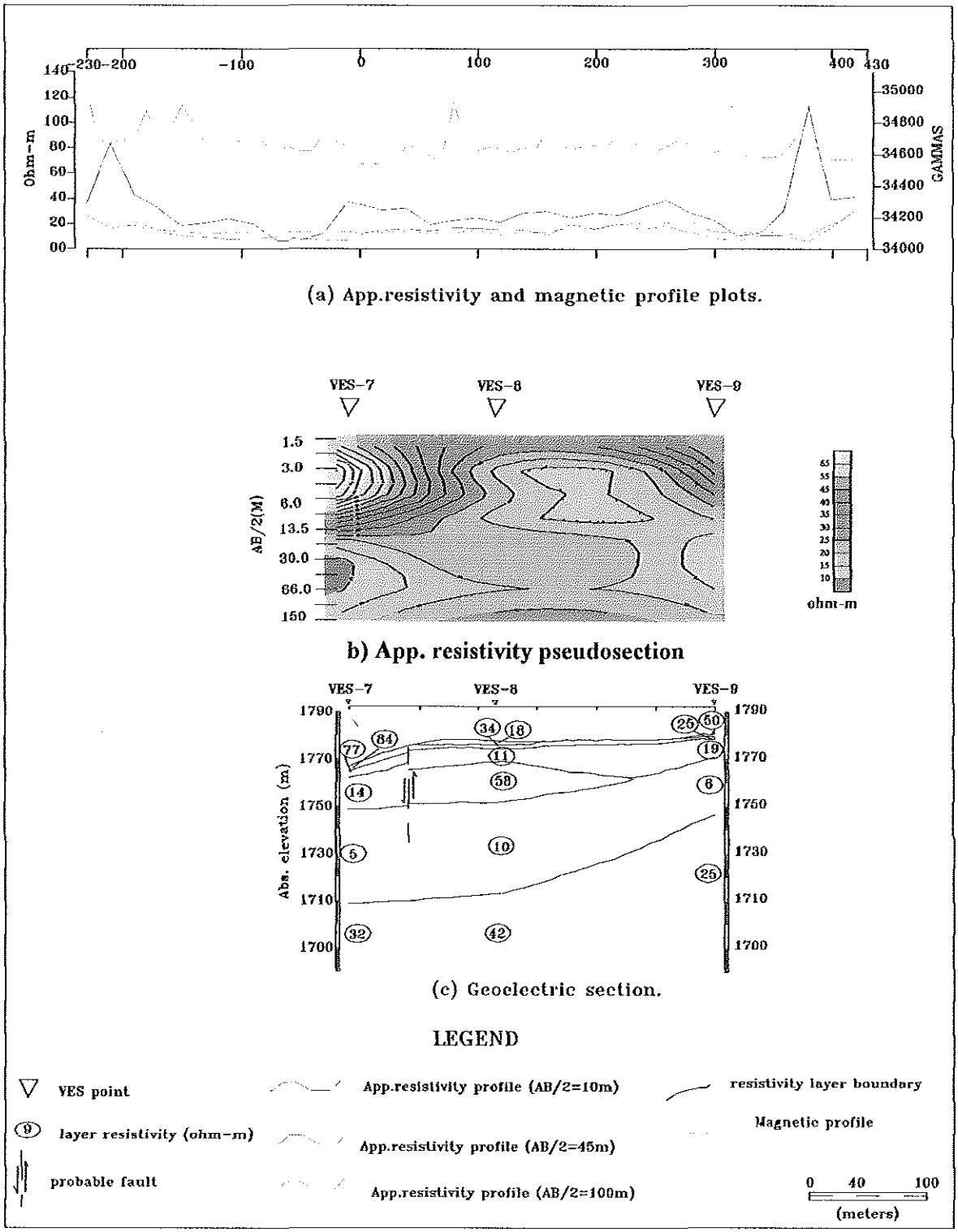

Fig. 26. Results of electrical and magnetic surveys along line-4, Kebele 02, Bonga.

Line-10

The resistivity pseudo-section along profile 10 (Fig. 27b) reflects the generally high, low, and then high type of resistivity distribution depth wise. This vertical trend of resistivity distribution is a general characteristics of the interpreted pseudo-sections so far along the selected lines that are thought to be representative of the survey lines on the area. The alternating distribution of resistivity values with depth is again as that of the previous cases to be due to increase and decrease in water saturation that results from heterogeneity and varying degree of weathering/fracturing of the rock masses involved in the area.

The geo-electric section along line 10 (Fig. 27c) illustrates 4 electrical stratification along the profile with an additional electrical layer beneath the western flank of the line.

The 165 and 375 m locations, where the two streams running with in the survey area cross the line (line 10), are identified by sharp resistivity peaks observed on the AB/2=10 m level resistivity plot (Fig. 19a). In addition to this there is also a magnetic gradient at about 165 m location as illustrated on the magnetic plot (Fig. 19a). This resistivity and magnetic signatures could be interpreted as a possible structure (fault) that could have association to the beds of the streams that follow mostly week zones. This interpretation is also supported by the result of low refractor velocity (1400 m/s) response obtained in particular at the 165 m location, where the western stream cross the line (Fig. 17).

On the geo-electric section (Fig. 27c) the top geo-electric layer exhibits a nearly a uniform range of resistivity values (57-85 ohm-m) with thicknesses varying from 1 - 5 m. The second

geo-electric layer with resistivity values ranging from 189 - 232 ohm-m and respective thicknesses varying from 2 - 4 m is registered on a extreme western and eastern ends of the profile. A third geo-electric layer to the west of the central part that correspond to a second layer of the central part is represented by a 38 & 52 ohm-m resistivity value and maximum thickness of 7m around the centre. This layer is pinches out from both the left and right hand side of the western stream (at 180m location) and completely vanishes at the location of the eastern stream (at 380m location).

The next geo-electric layer has the least resistivity range (716 ohm-m), maximum thickness of 60 m beneath both the eastern and western flanks of the central part and a minimum thickness of 25 m beneath the central part all along the profile. The bottom geo-electric layer has a uniform resistivity (56-62 ohm-m) all along the profile except at the extreme west where it suddenly rises to 275 ohm. Furthermore, the boundary of this layer and its the overlaying layer occurs at relatively uniform depth level (1690 m above sea level) and dips downwards (to a depth level of 1670 m above sea level) beginning from about the location of VES- 20 while moving towards west along the profile (Fig. 27c).

Line- 13

The resistivity distribution depicted by the pseudo-section along line 13 (Fig. 28b) shows, the high, low and then high trend of resistivity distribution with depth similar to those of the previous pseudo-sections. Apart from this, the unique resistivity distribution displayed by the

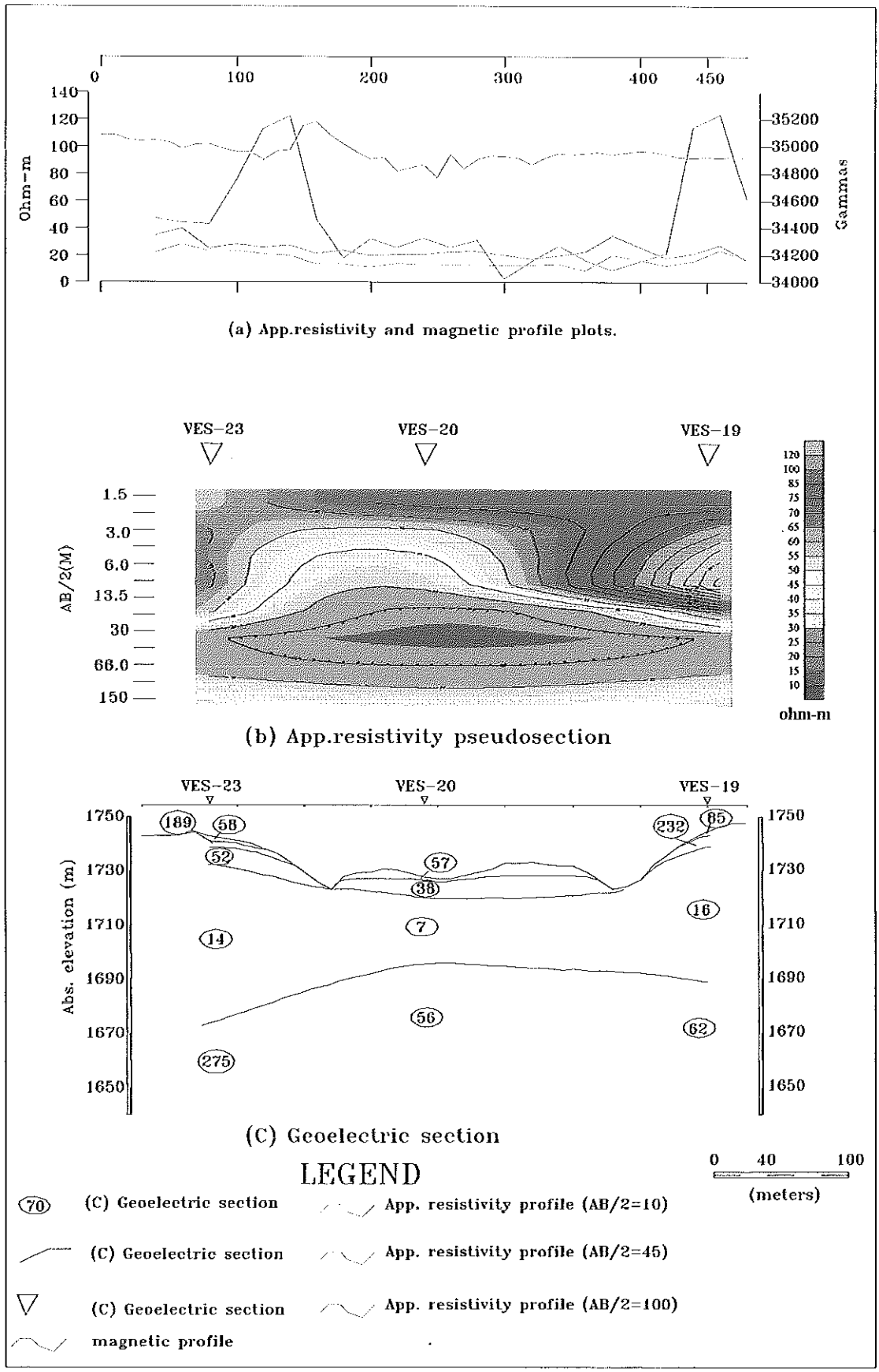

Fig. 27. Results of electrical and magnetic surveys along line-10, Kebele 02, Bonga.

pseudo section along line 13 is the appearance of a relatively lower and narrow (extending from location 340 m to 420 m) resistivity layer that interrupts the top high resistivity layer. This low resistivity layer corresponds to a near surface vertical discontinuity probably a vertical fault that is also evidently distinguished on the magnetic plot (Fig. 28a) by a local high magnetic response, furthermore, this all is distinguished by an attenuated surface topography gently dipping lows towards the river bed and highs on either side of it. The heterogeneity of rocks by deposition of surface water flow on the deeping topography, makes the top surface is easily susceptible for land slide activity. The high resistivity shift at 550m level (Fig. 24a) also reflects the presence of a possible structural feature (fault).

The geo-electric section along line 13 (Fig. 28c) signifies a general subdivision of the subsurface along this profile characterised by four geo-electric layers with a rang of resistivity values 20-52 ohm-m for the 1st layer, 50-102 ohm-m for the 2nd layer, 11-15 ohm-m for the 3rd layer and 41-121 ohm-m or the 4th layer. An exception to this general subdivision is, the appearance of an additional layer that makes the number of layers to five at the extreme north of the profile beneath VES-16 beginning from the 550 m location.

A top and thin (less than 1.6m) geo-electric layer with resistivity values varying from 2 - 20 ohm-m overlies a relatively thicker (515 m) and uniform resistivity value of insignificant variation (from 50 - 56 ohm-m only) layer which disappears at about 470 m location corresponding to the location of the stream across the line.

The second geo-electric layer beneath the profile to the right hand side of the stream extends up to the location of the suspected fault at 550 m location. Based on the results of the

generated geo-electric and pseudo-sections, magnetic and resistivity plots (Fig. 28) it is characterised by 102 ohm-m resistivity and 2m thickness, extending upto the probable fault at 550 m level. To the north of the fault the second layer becomes thicker and attains about 10 m. The relative variation in thickness of this layer (2 m) to the left and (10 m) to the right of the 550 m location signifies the vertical displacement (8 m) of the rock masses forming the suspected fault at this location. The horizontal variation in resistivity evident on the left and right hand side of 1st layer, on the left and right hand side of the 2nd layer, and on all corresponding layers at 550 m location signifies the appearance of different geologic units that constitute the suspected fault or weak zone.

Of all the distinguished layers beneath the profile to the left of the 550 m location the 3rd layer is identified with a range of the least resistivity values (9 - 15 ohm-m), thickness (40 -63 m) and depth of occurrences (1-16 m) from surface. Correspondingly the least resistivity layer beneath the profile to the right of the 550 m location is identified with the least resistivity value 27 ohm-m, thickness about 80 m and depth of occurrence 35 m from surface.

The bottom geo-electric layer to the left of the 550m location attains a maximum resistivity value (about 120 ohm-m) at about 250 m location and decreases both to the left and right of this location, the minimum resistivity value (41 ohm-m) occurring beneath VES-13. The corresponding bottom layer beneath the profile to the right of the 550m location attains a 140 ohm-m resistivity.

To generalise the interpretation of the resistivity result obtained in the area, it is possible to classify the near surface stratigraphy of the area into three major electrical sequences. The top relatively higher resistivity values is due to the unconsolidated colluvial soil and volcanic

formation that is affected by cracking, subsidence and high degree of weathering which are factors that hamper the propagation of current through the formation. The next sequence is a volcanic formation that is less weathered than the overlaying high resistivity sequence but it is highly fractured and water saturated which cause easy current flow that results low resistivity values. The bottom relatively fresh and homogeneous volcanic formations (dominantly basalt) are characterised by relatively uniform higher resistivity values. The resistivity increase at depth is due to the decrease in rate of fracturing /weathering in turn that decreases the porosity which is the responsible factor for the follow of current in rocks.

This alternating trend of vertical resistivity distribution is a general characteristics of the interpreted pseudo-sections and geo-electric sections so far along the selected lines that are thought to be representative of the survey lines in the area. This alternating distribution of resistivity values with depth as those of the previous cases is thought to be due to the increase and decrease in water saturation, heterogeneity of rocks and degree of weathering of the involved rock masses.

4.4 Zonal classification of the study area based on the investigation results

Based on the geophysical investigation results that are constrained by surface geological mapping the study area is classified into five different zones (Z-1, Z-2,..., Z-5) shown in Figure 29 that also displays the location of the geophysicaly measured lines and the prominent surface geological rock units or structures of the area. This zonal sub-division is made to account for the relative stability of the different parts of the study area and identify the zones that are highly vulnerable to the occurred landslide and that may be susceptible for possible landslide occurrences in the future. Accordingly, a brief account of each zone is given here bellow.

Zone one (Z-1)

Zone one (Z-1) represents the northern part of the study area that is demarcated by the NNE-SSW oriented broken bold line, F2-F2' fault (Fig. 29). This zone is generally characterised by:

- relative magnetic responses of high, >34900 gamma, (western part), low, <34750 gamma (eastern part) and intermediate, from 34750-34900 gamma, (central part) intensity (Fig. 19),

- relative resistivity responses of high, >35 ohm-m, (western part), low, <20 ohm-m, (eastern part) and intermediate, from 20-35 ohm-m, (central part) magnitude (Fig 22) at the AB/2=10

m (Fig 22) level and generally higher resistivity value at both the AB/2=45 m (Fig. 23) and AB/2=100 m (Fig. 24) levels,

- relative high bottom refractor velocity (>3000 m/s) obtained at the depth of 15 - 22 m (Fig. 13 & 14).

Based up on the above geophysical responses it is inferred that the surface rocks that extend to a depth of 7 m (the maximum investigation of AB/2=10 m level) seem to be more consolidated (probably an agglomerate of basaltic material covered by a very thin layer of colluvial soil) in the western part in comparison to that of (basaltic material covered by relatively thicker colluvial soil) on the eastern part overlaying a basaltic material. The results of seismic and geo-electric sections, pseudo-sections and magnetic and resistivity plots generated along line 10 and 13 that partially pass along this zone are consistent with that of the geophysical maps results discussed above (Fig. 17, 18, 27 & 28). All this conditions indicates that zone one is relatively stable, however, as it goes north where the topographic gradient increases its relative stability proportionally decreases.

Zone two (Z-2)

Zone two (Z-2) represents the northeastern part of the study area that is demarcated by the NNW-SSE oriented broken bold line, F4-F4' fault (Fig. 29). This zone is generally characterised by:

- relative magnetic responses of generally intermediate intensity (Fig. 19)

- relative resistivity responses of generally high magnitude at the AB/2=10 m (Fig 22) level and generally lower resistivity value at both the AB/2=45 m (Fig. 23) and AB/2=100 m (Fig. 24) levels.

- relatively intermediate refractor velocity (from 2000- 3000 m/s) response obtained at the depth of 10-20m (Fig. 13 & 14).

Based on the above geophysical responses it is inferred that the surface rocks that reside in this zone seem to be unconsolidated and unsaturated colluvial soil overlaying the highly fractured and possibly weathered and water saturated volcanic formation (probably basalt) situated in the area. The results of seismic and geo-electric sections, pseudo-sections and magnetic and resistivity plots generated along eastern part of line 10 that pass along this zone are consistent with that of the geophysical maps results discussed above (Fig. 17 & 27). The non-availability of landslide features in conjunction with the present results of the integrated geophysical surveys this zone is classified as relatively stable zone.

Zone three (Z-3)

Zone three (Z-3) represents the southern part of the study area that is demarcated by the NNW-SSE oriented broken bold line, F1-F1' fault (Fig. 29). This zone is generally characterised by:

- relative magnetic responses of high (southern part), low (northern part) and intermediate (central part) intensity (Fig. 19),

- relative resistivity responses of high magnitude at the AB/2=10 m (Fig 22) level and generally intermediate to low resistivity value at both the AB/2=45 m (Fig. 23) and AB/2=100 m (Fig. 24) levels.

- relative refractor velocity of low ,<2000 m/s, (south eastern part) and intermediate (eastern part) response at a depth of 10-15 m (Fig. 13 & 14)

Based up on the above geophysical investigation results it is inferred that the near surface rocks seem to be unconsolidated formation (dry residual soil of basaltic origin) in the southern part that compositional change unsaturated colluvial soil in the northern side. The underlying formation is thought to be weathered and fractured volcanic rock (most probably basalt) that show decrease in degree of weathering and fracturing toward west and depth wise. The results of seismic and geo-electric sections, pseudo-sections and magnetic and resistivity plots generated along eastern part of line-1 that pass along this zone are consistent with that of the geophysical maps results discussed above (Fig. 15, & 25).

This basaltic zone which is overlain by residual and colluvial soils affected by weathering is vulnerable for landslide activities, therefore, it could be identified as less unstable zone.

Zone four (Z-4)

Zone four (Z-4) represents the western and southwestern part of the study area that is demarcated by the NNE-SSW oriented landslide scarp (Fig. 29). This zone is generally characterised by:

- relative magnetic responses of generally from intermediate to high intensity (Fig. 19),

- relative resistivity responses of low (southern part) and intermediate to high (northern part) magnitude at the AB/2=10 m (Fig 22) level and intermediate (northern part) and dominantly low (southern part) resistivity value at both the AB/2=45 m (Fig. 23) and AB/2=100 m (Fig. 24) levels.

- relative refractor velocity of low (northern part), intermediate (central part) and high (southern part) responses at a shallower depth (6-12 m) at north and become deeper (17-25 m) at southern part (Fig. 13 & 14)

Based up on the above geophysical responses it is inferred that the near surface rocks at the northern part of this zone seem to be water bearing weathered and fractured basalts, where its degree of saturation increases depth wise. Whereas the southern part is thought to be thick and water bearing formation (most probably an agglomerate of coluvial soil dominantly basaltic origin) that is underlying by a homogeneous water bearing fractured formation (most probably basalt) that is continuous depth wise all throughout the area beneath this zone. The results of seismic and geo-electric sections, pseudo-section and

magnetic and resistivity plots generated along the western part of line-1 that pass along this zone are consistent with that of the geophysical maps results discussed above (Fig. 15, & 25).

Z-4 is relatively stable zone despite the NW-SE trending active landslide scarp that serves as the eastern boundary of the zone and the relatively smooth topography in the southern part is also additional factor to categorize the zone as relatively stable zone.

Zone five (Z-5)

Zone five (Z-5) represents the central part of the study area that is demarcated by the broken lines that run NNE-SSW (F2-F2' fault) in the north, NNW-SSE (F3-F3' fault) in the south NNW-SSE (F4-F4' fault) in the east and a N-S line that demarcates the western boundary of the survey area through the 100W meridian (Fig 29). Most of the geophysical survey lines considered in this study are included within this zone. This zone is generally characterised by:

- relative NNW-SSE trending magnetic responses of low (western part), high (eastern part) intensity that is bounded by F1-F1' & F2-F2' probable faults from the northern and southern directions respectively and a nearly E-W trending intermediate magnetic responses at the centre and at the northern boundary of the zone along line 10 (Fig 19 & 21),

- relative resistivity responses of high (western part), low (central part) and intermediate to low (eastern part) magnitude at the AB/2=10 m (Fig 22) level and generally NNE-SSW oriented central low flanked by intermediate resistivity value on both the AB/2=45 m (Fig. 23) and AB/2=100 m (Fig. 24) levels.

- relative bottom refractor velocity low (between line 9 and 10, at the centre that cross lines 6 & 13, at the east that crosses lines 2, 3, 4 & 5 and some sporadic lows at he centre and southern part along line 2), high (between line 8 & 9 and line 1 & 4) and intermediate (the rest of the central part) with refractor depth of 5-30 m (Fig. 13 & 14)

Based on the above geophysical results the occurrence of sporadic lows and highs particularly for the responses at the surface geological units is thought to be due to complex nature of the rock units that reside in zone five. The boundary along which a transition from high to low or vice-versa magnetic responses (Fig. 19, 20 & 21) and resistivity responses (particularly at the AB/2=10 m level) marks a contact (horizontal/vertical contact) between surface rocks of the same or different types with varying water saturation. The occurrence of such boundaries is closely associated with the occurrence of the active landslide scarps shown on the engineering geology map (Fig. 3). The implication of the integrated geophysical results when constrained by the geologically mapped geological units of the study area is that the unstable zones that favour occurrence of landslide are those that exhibit a transition from high to low of the geophysical responses revealed on the respective geophysical maps. In particular the geophysical responses that reveal these phenomena when given in order seem to come from resistivity, magnetic and seismic. The results of seismic and geo-electric sections, pseudo-sections and magnetic and resistivity plots

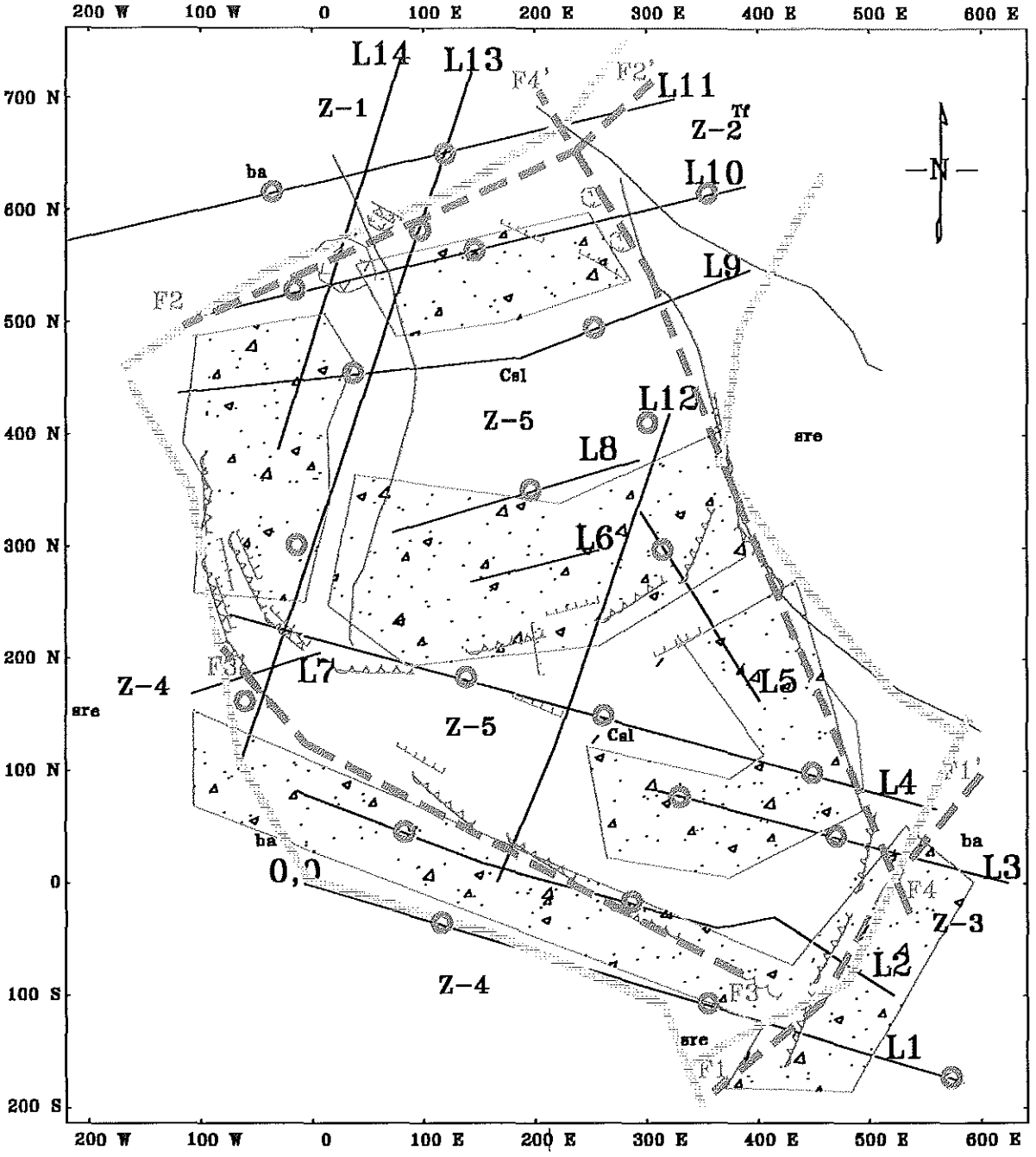

Fig. 29 Combined Interpretation map of kebele 02, BONGA

Legend

Tf Weathered tuff

ba Moderately weathered basalt

sre Residual soil

Csl Colluvial soil

Active slides

Lithologic contact determined both geophysically and geologically

cracking/fracturing

Active land slide scarp

Active zones of land slide as obtained from the combined geophysical data

F1 F1' Geophysically interpreted fault

Z-1 interpretation zone - 1

perennial stream

L7 Geophisical profils

VES points

25 0 50 100 (metres)

generated along line 4, 10 and 13 that mostly passes along this zone are consistent with that of the geophysical maps results discussed above (Fig. 16, 17, 18, 26, 27 & 28).

All these physical conditions and the geological manifestations lead to categorise zone five as most unstable zone. However there is a relatively stable zone within zone five (Z-5) bonded by central and northern active slide zones known by their relatively high refractor velocity, at a depth of 8 to 14m (Fig. 13 & 14).

Eventhough, the area is classified in five different zones attending engineering geological, hydrogeological and structural conditions (Fig. 29) based on relative physical responses, the casualty area as a whole is not favourable for urban development.

CHAPTER 5

DISCUSSIONS, CONCLUSIONS, AND RECOMENDITIONS

5.1 Discussions

The absence of any attention seeking (mineral or any related conditions) in the study area (the Bonga town and its surrounding) makes the area in lack of sufficient geological or any other related earth science references for correlation with the current engineering geological and geophysical results.

Due to the slope gradient and nature of soils and rocks covering the area along with shallow ground water condition the entire landslide process is significantly augmented. The groundwater table of the Bonga town is generally shallow (5 - 25 m) as confirmed by depth measurement of hand dug wells for potable water by the residents. This shallow groundwater depth is consistent with the depth obtained by the VES investigation results, identified as the boundary of the least resistivity layer (relatively highly water saturated material and lower resistivity value) and the overlying unconsolidated loose material (relatively lower water saturation and higher resistivity value) displayed on all the geo-electric sections along the interpreted lines (Fig. 25, 26, 27 & 28) under this study. The thickness of the unconsolidated formations (relatively lower velocity, <2000 m/s), 5-32 m,

obtained from the seismic refraction seismic result (Fig. 15, 16, 17 & 18) is also found to bear a fair correlation with the above mentioned water table depth.

Landslide occurrences investigations elsewhere have shown that the groundwater level of a landslide area which determines the gravitational weighting of a landslide body, the supporting hydrostatic pressure and the hydrodynamic pressure of seepage flow are the major factors that affect the stability of the landslide body (Bogoslovsky, 1977). The saturation of unconsolidated colluvial and alluvial soil and the highly weathered volcanic formations of basaltic origin from recharge of groundwater system and the high intensity and long term rainfall reported (Tesfaye Chernet, 1988) in the area are determined to have a major contribution to landslide processes of the Bonga town by wetting and increasing the volume that introduces imbalance between the shearing and resisting forces that generate instability.

Rocks affected by weathering loose the shearing stress as a result cracks are formed which facilitate the landslide process (Maslov, 1987; Scheidegger, 1988). The integrated geophysical and geological results of the Bonga town have shown the physical characteristics of the rocks (of the same or different types) that reside the study area are highly altered due to weathering, fracturing and water-saturation. This alteration that is determined to be dominantly associated with the near surface formations above the groundwater table seems likely to form favourable grounds for the landslide occurrences of the area (Fig. 29). Furthermore, the association of the landslide affected zones with the geophysically and geologically identified structural features (faults/contacts) has shade light

regarding the unstable condition the area as whole to favour the already occurred landslide activities and those ones that may be anticipated in the future.

Human interference by removal of lateral support (such as deforestation, unplanned/uncontrolled infrastructures, etc) and thereby increasing shearing force through different constructions is a contributing factor that enhances landslide phenomena of a landslide prone area (Jovanovic, 1988). Since the study area (the Bonga town) is a rapidly developing zonal administration centre where extensive construction activities are underway, these activities may also have a bearing (however small) in aggravating the recent landslide phenomena.

On a regional basis, the study area lies within a low seismic risk zone (ZONE 1) as identified on the seismic risk zone map of Ethiopia (GOUIN, 1976) indicating that earthquake activities which have a potential to trigger and aggravate landslide phenomena is minimal.

Of all the above factors, the nature of the topography, which dips in a general S-N direction at with a sufficiently high gradient (particularly, at the eastern and northern parts) favours landslide activities to become hazardous phenomena for the area as a whole.

5.2 Conclusions

The geophysical methods conducted in the Bonga town to investigate the landslide-affected site (Kebele 02) have outlined very important results in understanding the thickness of the sliding mass body, the major cause(s) of the landslide phenomena and the relative stability of the different zones that constitute the area. Based on these investigation results the following are the conclusions that may be drawn.

- Lithologically, the landslide is mainly related with the top colluvial layer with varying degree of saturation, consolidation and topographical gradient, of which the degree of water saturation and the topographic gradient are thought to be the major contributing factors that aggravate the landslide phenomena. The top layer that favours landslide occurrence in the study area is determined to have an average thickness of about seven-meter. Underlying this fresh to highly weathered, fractured and water saturated volcanic sequence is present, which is generally identified by very low resistivity and intermediate refractor velocity.

- The landslide phenomena is intensive at places where occurrences in space of shallow contacts (horizontal/vertical) of loose colluvial deposits and the underlying water saturated rock masses (from the geophysical results) and structural disturbances (geophysical and geological) are most frequent in the study area under consideration.

- The geophysical results have identified four main possible structural trends (faults): F1-F1', F2-F2', F3-F3' and F4-F4'. These geophysicaly inferred structural features are in good correlation with the occurrences and orientation of the geologically mapped active landslide scarps in the area.

- The reported high intensity and long duration rainfall of the area that saturates the top soil and also causes the ground water level to rise is the main landslide triggering factor. This is simply due to the imbalance it creates between the shearing and resistance force by reducing the latter.

- From the regional hydrogeology and the current geophysical investigation (particularly electrical) the study area lies over thick water saturated zone. The sounding result indicates that the thickness of saturated zone reaches 80 m that is consistent with the depth of the ground water level in the study area that varies from 5 to 25 m.

- Based on the results of the geophysical and geological data the relative stability of the studied area with regard to the lithological, structural, geophysical, hydrogeological conditions is classified into five zones of which Zone five (Z-5) is determined to be the most unstable one that favour landslide occurrences. However, from the point of view of

urban development, the whole area may not be favorable for infrastructure development and is unlikely to be chosen as a settlement site.

5.3 Recommendations

Based on the outcome of this study, the following recommendation are forwarded:

- It is advisable not to encourage any large-scale infrastructural developments/constructions that can most probably cause active shearing force by disturbing the equilibrium condition beyond the capacity of the resisting force.

- Eventhough the area is outside of seismically active zone, it has a regional unstability problem. Therefore, it is important to have timely information regarding the seismicity of the area.

- Three to four shallow boreholes (up to 40 m depth) are proposed to be sunk at selected locations that are most affected by the landslide phenomena as determined by the results of the present survey. The knowledge that will be acquired about the subsurface

conditions of the study area from the borehole data is of critical importance to constrain the current geological and geophysical results in the process of obtaining reliable information regarding the subsurface condition of the area. The constraints that come out from the bore hole data can also impose conditions for a reinterpretation of the present geophysical data and thereby apply corrections to any wrong interpretations that might have been made if their occurrence is confirmed. The occurrence of wrong interpretations of geophysical data without the constraint of independent actual data that reveal the ground truth is likely because of the ambiguities (limitations) that are naturally involved with geophysical methods in resolving geological problems.

- The concerned federal or regional government organization officials (including planners) are advised to find a suitable alternate sites and also work very closely with the inhabitants towards mitigating the currently prevailing geohazard situation by taking preventive measures, like constructing retaining walls on the side of road cuts, constructing properly designed drainage lines, planting trees, avoid cutting trees, etc.

BIBLLOGRAPHY

Atkins, W.P., The elements of physical chmeistry, Great Britin, 1992

Bilgrami, S.K. Fundmentals of Botany, New Delhi 1978

Cotton, Albert, F. Basic inoganic chemistry, united states of america 1975

John l. Gitteman., Carnivor Behavior ecology and evolution, New yourk, 1989

Hartl, Daniel, L., A primer of population Genetics, U.S.A.,

Pozdnyakov V.I., Vurse's hand book, Russian, 1984.

Peebles, P.J.E., Principles of phusical cosmology, Singapore, 1980.

Michel, F. Curtis, Theory of nuetron star magnetospheres, London, 1991

Seneci, Pierfausto., Solid-phase synthesis and combinatorial techniologies, united stes of america, 1960.

Schreiber, Elmar., Femtose cond Real-time spectros copy,of small molecules and clusters New york, 1998.

References

Archie, G.E., 1942. The electrical resistivity log as and aid in determining some reservoir charactersitics. Thrans. Am. Inst. Min. Metall. Engrs., 146, 54-62.

Berker, R.D. & Worthington, P.F., 1973. Some Hydrogeophysical properties of the Bunter sandstone of Northeast England. Geoexploration, 11, 151-170.

Bogoslovsky, V.A. and Ogilvy, A.A., 1977. Geophysical methods for the interpretation of landslide. Geophysics Vol. 42, p. 562-571.

Cecchi, M.M., Marchisio, M. and Montani, C., 1977. A methodological study about the quantitative interpretation of geophysical survey results. Geophys. Prospect., 25: 606-607 (abstr.).

Dobrin, M.B. and Savit, C.H., 1988. Introduction to geophysical prospecting. McGraw Hill. Newyork.

Ebert, A., 1943. Grundlagen zur Auswertung geoelektricher Tiefenmessungen. Beitr. Angew. Geophys. 10: 1-17

GEOSOFT Mapping system, 1992. Toronto, Canada.

Gouin, P., 1976. Seismic zoning in Ethiopia. Bulletin of the geophysical observatory, No: 17.

Gurvich, I., 1972. Refraction seismic prospecting. Mir publishers, Moscow.

Inman, J.R., Ryu, J. and Ward, S.H., 1973. Resistivity inversion. Geophysics, 38: 1088-1108.

Johansen, H.K., 1977. A man/computer interpretation system for resistivity soundings over a horizontally stratified earth. Geophys. Prospect., 25: 667-691.

Kearey, P. and Brooks, M., 1979. An introduction to geophysical exploration. London.

Keller, G.V. and Frischnecht, F.C., 1966. Electrical methods in geophysical prospecting. Pregaman, Oxford.

Koefoed, O., 1968. The application of kernel function in interpreting resistivity measurement. Gerbruder Borntraeger, Berlin.

Koefoed, O., 1970 A fast method for determining the layer distribution from the raied kernel function in geoelectrical soundings. Geohys. Prospect., 18: 564-570.

Koefoed, O., 1979. Geosounding principles, 1. Resistivity sounding measurements. Methods in geochemistry and geophysics. Elsevier, Amsterdam.

Maslov, N.N., 1972. Basic engineering geology and soil mechanics. Mir publishers, Moscow.

Marquardt, D.W., 1963. An algorithm for least-squares estimation of nonlinear parameters. J. Soc. Ind. Appl, Math., 11: 431-441.

Marsden, D., 1973. The automatic fitting of a resistivity sounding by a geometrical progression of depths. Geophys. Prospect., 21: 266-280.

Meinardus, H.A., 1970. Numerical interpretation of resistivity soundings over horizontal beds. Geophys. Prospect., 18: 415-433.

Megesha Tefera, Tadiwos Chernet and Workineh Haro, 1996. Geological map of Ethiopia, 2nd edition, Regional geology department, Ethiopian Institute of Geological Surveys, Addis Ababa.

Moges Tigabe, 1991. Some studies on computer- assisted interpretation of resistivity sounding data. Indian Institute of Technology, Department of geology and geophysics, Kharagpur (M.Sc. thesis).

Moonery, H.M. and Wetzel, W.W., 1956. The potentials about a point electrode and apparent resistivity curves for a two-, three-, and four-layered earth. University of Minnesota Press, Minneapolis, Minn., 146 pp.

Ng, C.W.W. & Shi, Q., 1998. Influence of rainfall intensity and duration on slop stability in unsaturated soils. Quarterly journal of engineering geology, V. 31, P. 105-113.

Nettleton, L.L., 1976. Gravity and magnetics in oil prospecting. McGRAW-HILL, New York.

Orellana, E. and Mooney, H.M., 1966. Master Tables and curves for Vertical Electrical Sounding over Layered Structures. Interciencia, Madrid, 34 pp.

Pekeris, C.L., 1940. Direct method of interpretation in resistivity prospecting. Geophysics, 5: 31-46.

Rijkswaterstaat, 1969. Standard Graphs for Resistivity Prospecting. European Association of Exploration Geophysicists, The Hague, 4 pp.

Sarmiento, R., 1961. Geological factors influencing porosity estimates from velocity logs. Bull. Am. Ass. Petrol. Geols., 45, 634-644.

Scott, J.H., Lee, F.t., Carroll, R.D. & Robinson, C.S., 1968. The relationship of geophysical measurements to engineering and construction parameters in the straight creak tunnel Pilot Bore, Colorado. Int. J. Rock Mech. Min. Sci. 5, 1-30.

Sjogrern, B., 1984. Shallow refraction seismic. Chapman and Hall, USA.

Slichter, L.B., 1933. The interpretation of resistivity prospecting method for horizontal structures. Physics, 4: 307-322.

Smith, W.D.M., 1970. Petrophysical relationships from the western Canada area. Log Analyst, 11, No.5, 3-16.

Stagg, K.B. & Zienkiewicz, O.C., 1968. Rock mechanics in engineering practice. London

Telford, W.M., Sheriff, R.E. and Geldart, L.P., 1980. Applied geophysics. Cambridge, London.

Tesfaye Chernet, 1988. Hydrogeological map of Ethiopia. Ethiopian Institute of Geological Surveys, Addis Ababa.

Van Nostrand, R.g. and Cook, K.L., 1955. Apparent resistivity for dipping beds - a discussion. Geophysics., 20: 140-147.

Zohdy. A.A.R., 1965. The auxiliary point method of electrical sounding interpretation and its relationship to the Dar-Zarrouk parameters. Geophysics, Vol. 30, P. 644-660.

Zohdy, A.A.R., 1974. Automatic interpretation of Schlumberger sounding curves. Geol. Surv. Bull. 1313-E. U.S. Government Printing Office, Washington, 71 pp.